catalysts

MDPI

Article

Selective Conversion of Glycerol to Acetol: Effect of the Preparation Method of CuAl Catalysts and Reaction Phase

Francisco Maldonado-Martín, Lucía García *, Joaquín Ruiz, Miriam Oliva and Jesús Arauzo

Thermochemical Processes Group (GPT), Aragon Institute of Engineering Research (I3A), Universidad de Zaragoza, Mariano Esquillor S/N, 50018 Zaragoza, Spain; fmaldonado@unizar.es (F.M.-M.); jruizp@unizar.es (J.R.); miroliva@unizar.es (M.O.); jarauzo@unizar.es (J.A.)

* Correspondence: luciag@unizar.es

Abstract: A group of CuAl catalysts were synthesized with a Cu/Al molar ratio of 1:1 using different preparation methods: coprecipitation, surfactant assisted coprecipitation, polymeric precursor, and self-combustion and then screened for the selective dehydration of glycerol to acetol. The catalysts were employed in glycerol conversion at the same temperature (227 °C) in two different laboratory-scale systems, the first one at atmospheric pressure (gas phase) and the second one in a pressurized system at 34 absolute bar (liquid phase). The preparation method of the CuAl catalysts influenced the carbon yield to liquids and acetol selectivity. However, the reaction phase had a greater influence than the preparation method of the catalyst. In the gas phase, the carbon yield to liquids reached values above 40% and the carbon selectivity to acetol was higher than 90%. The highest acetol yield, 462.6 $mg_{acetol}/g_{glycerol}$, was obtained with the CuAl catalyst prepared by the surfactant-assisted coprecipitation method. This study provides a new perspective on catalyst design by highlighting the crucial role of preparation techniques in determining CuAl catalyst performance in the liquid and gas phases.

Keywords: CuAl catalysts; catalyst preparation; liquid phase; gas phase; glycerol; acetol

Academic Editor: Sergio Nogales Delgado

Received: 7 March 2025
Revised: 28 March 2025
Accepted: 31 March 2025
Published: 2 April 2025

Citation: Maldonado-Martín, F.; García, L.; Ruiz, J.; Oliva, M.; Arauzo, J. Selective Conversion of Glycerol to Acetol: Effect of the Preparation Method of CuAl Catalysts and Reaction Phase. *Catalysts* **2025**, *15*, 348. https://doi.org/10.3390/catal15040348

1. Introduction

Fossil fuels, the primary energy source for decades, are highly polluting and contribute to climate change. Their limited availability [1] further underscores the need for renewable alternatives. OPEC predicts the global fuel demand will rise to 109.4 million barrels per day by 2040, with diesel demand reaching 5.7 million barrels daily [2]. To reduce reliance on petroleum, researchers are exploring renewable options like biomass valorization [3], hydrogen production [4], and biofuels [5].

Biodiesel, a promising biofuel, is produced via the transesterification of triglycerides from sources like vegetable oils and animal fats. It offers advantages such as lower emissions, non-toxicity, and high lubricity [2,6]. However, its high production costs hinder its industry growth. There are several paths to decrease the production costs of biodiesel [7,8], among them being the development of new technologies capable of valorizing biodiesel production's by-products. The most important byproduct in terms of volume is glycerol, which is produced at 100 kg per ton of biodiesel [9]. With the biodiesel industry expanding, glycerol production is expected to grow significantly [10].

Glycerol, or 1,2,3-propanetriol, has diverse applications in industries like food, cosmetics, and pharmaceuticals [11]. It is also used in concrete additives and aviation fuel production [5]. The surplus of glycerol from biodiesel production has spurred research into its valorization through processes like reforming [4,11], hydrogenolysis [12,13], and

dehydration [9]. The catalytic dehydration of glycerol, for instance, produces valuable compounds like acetol and acetone, which can be used to synthesize aviation fuels. The aldol condensation of biomass-derived furan compounds with ketones, such as acetone or acetol, produces liquid intermediates for jet fuels [5]. This technology offers a route to produce sustainable aviation fuels (SAFs), which could be relevant for CO_2 emissions' mitigation [14]. The production of SAFs by aldol condensation with acetol increases the utilization of this molecule [15].

Recent efforts focus on converting glycerol to acetol and acetone via catalytic dehydration and hydrodeoxygenation (HDO). However, producing acetone from glycerol is complex, requiring three steps: dehydration to acetol, hydrogenation to 1,2-propanediol (1,2-PDO), and further dehydration to acetone. This process demands multifunctional catalysts and yields low acetone selectivity (under 6%) [16].

The production of acetol and/or 1,2-PDO involves dehydration and dehydration–hydrogenation, conducted in either the gas (at atmospheric pressure) or liquid (at high pressure) phase. While most studies have focused on gas-phase glycerol dehydration/hydrogenolysis [17–21], the liquid-phase process requires less energy due to the absence of water vaporization and operates at moderate pressures (~34 bar) and low temperatures (227 °C) [13].

Catalysts play a critical role in both phases. Noble metals, although effective, are costly and exhibit low selectivity toward acetol [22,23]. Non-noble metals like Ni catalyze C-C bond cleavage, generating H_2, which lowers acetol selectivity due to hydrogenation to 1,2-PDO [24]. Co-based catalysts suffer from severe sintering and deactivation by coking [25,26]. In contrast, Cu-based catalysts preferentially cleave C-O bonds without breaking C-C bonds and with minimal hydrogen generation, making them suitable for acetol production [18,19,27].

The role of the catalyst support is relevant to increase the specific surface area, metallic dispersion, prevention of sintering, and control of product selectivity. Basic supports, such as MgO, CaO or ZnO, show low acetol selectivity [17]. Phosphate supports are negatively affected by the presence of water in the feed and promote the formation of acrolein due to the appearance of Brönsted-type acid centers [28]. Acidic supports with a high specific surface area, such as zeolite, achieve high glycerol conversion and selectivity to acetol [29]. However, in an aqueous-phase medium hydrolyze zeolite structure, neutral supports, such as SiO_2, are also hydrolyzed under hydrothermal conditions [30]. Al_2O_3 as a catalyst support of Cu catalysts in glycerol dehydration shows favorable properties due to metallic dispersion promoting [12,31,32] and glycerol activation [33] via hydrogen bridge formation with the hydroxyl groups of this molecule.

It has been reported that the effectiveness of Cu-based catalysts in glycerol dehydration/hydrogenolysis is greatly influenced by their structure and crystallinity [19]. In other words, the preparation method used for Cu-based catalysts, as well as the synthesis conditions, such as calcination, can significantly influence the performance of the catalysts. Severe calcination conditions, such as high temperatures, can negatively affect the properties of Cu-based catalysts. Additionally, the preparation method and calcination temperature have a strong impact on metal and support interaction. A strong copper–support interaction allows for the formation of crystalline phases capable of stabilizing the active phase, as previously was established by Zihui et al. [27].

The preparation method of the catalysts strongly influences the structural and catalytic properties of the obtained materials [34,35]. Dos Santos et al. [35] studied the effect of the preparation method for glycerol dehydration in the gas phase. They prepared the catalysts by two different methods: wet impregnation and a polymeric precursor. However, there is a lack of information on the effect of the CuAl catalyst preparation method on

important factors such as product selectivity, reaction mechanisms, and catalytic activity in glycerol dehydration.

Coprecipitation (CP) is a widely used preparation method that allows the obtention of highly-dispersed materials [15,34,36]. The catalysts obtained via this method tend to show low crystalline structures with a deficient metal–support interaction. However, the works of some researchers, such as Wolosiak-Hnat et al. [31], exhibit a remarkable metal–support interaction. This fact may be due to an aging step during the preparation that favored the metal diffusion. It is important to highlight the effect of the calcination temperature. Thus, a high calcination temperature leads to higher metal–support interaction, promoting the formation of spinel structure [37]. Basag et al. [37] concluded that calcination temperatures between 700–800 °C are required for promoting the metal–support interaction in CP CuAl catalysts. The higher Cu dispersion exhibited by these materials should have a positive effect on their catalytic activity. Furthermore, it could also be affected by the increased selectivity to 1,2-PDO due to an increase in acetol hydrogenation reactions [38].

The surfactant-assisted coprecipitation method (SACP) involves a coprecipitation method together with the use of a surfactant as a structure-directing agent. Several studies have investigated the effect of different surfactants, such as cetyltrimethylammonium bromide (CTAB), tetramethylammonium hydroxide, polyethylene glycol, and Pluronic P123, on several reactions, such as methanol synthesis, methanol steam reforming, and CO_2 reforming [39–42]. The use of a structure-directing agent should result in materials with controlled porosity. This should improve conversion and selectivity compared to the traditional CP method. However, there are few studies where the catalytic dehydration of glycerol in the aqueous phase is studied.

Charisiou et al. [43] previously investigated the catalytic steam reforming of glycerol employing SACP catalysts. Using Al-based catalysts and temperature ranges between 400–750 °C, researchers were able to achieve maximum values of carbon selectivity to acetol and acetone of 30% and 35%, respectively. This demonstrates the potential of catalytic dehydration of glycerol in the gas phase using SACP catalysts, making it an area of great interest for further study [43]. This also opens up an area of great interest for liquid phase research.

Polymeric precursor (PP) and auto-combustion (AC) preparation methods involve a combustion step that strongly affects metal dispersion and intermetallic interaction. PP is a widely studied method [34,35,44–46] that involves the chelation of metallic cations by citric acid in a water solution. Then, the remaining carboxylic acid function is polyesterified with ethylene glycol. This chelation step allows obtaining a homogeneous resin that promotes metal interaction. Moreover, the increment of temperature during the chelation step also favors metallic interactions.

The AC preparation method is a straightforward technique that can produce solid materials without the drying step. This approach yields homogeneous materials with a robust intermetallic interaction. Additionally, due to its simplicity and low consumption of raw materials, AC synthesis is highly cost-effective, making it ideal for scaling and industrial use in the preparation of catalysts. This method consists of the spontaneous combustion of an aqueous mixture containing the combustion agent (citric acid, urea, glucose, or glycine) and the metal nitrate precursors [47–50]. This combustion step is responsible for the intense metal–support interaction. These two preparation methods, PP and AC, are characterized by increased metal–support interaction. This increased interaction is expected to decrease metal dispersion, which in turn reduces the activity of these materials. However, this phenomenon could also increase acetol selectivity.

CuAl catalysts are promising materials for glycerol conversion to value-added products such as acetol/1,2-PDO. These products can be used as intermediates for the produc-

tion of sustainable aviation fuel (SAF). To the best of our knowledge, there is a lack of information about the influence of the preparation methods of CuAl catalysts on glycerol dehydration/hydrogenolysis, especially in the liquid phase. We aim to study the effect of the preparation method of CuAl catalysts on these processes. For this purpose, CuAl catalysts have been prepared by four different preparation methods: AC, CP, SACP, and PP. In addition, experiments have been carried out in the liquid and gas phases. Characterization of the calcined and the used catalysts determined relevant information to explain the catalytic performance and catalyst stability in the reaction medium.

2. Results and Discussion

2.1. Catalyst Characterization

2.1.1. Metal Content and Textural Properties

Table 1 shows the metal content in the calcined catalysts determined by ICP-OES. The metal content is expressed as the molar ratio Cu/(Cu + Al) × 100. An adequate agreement is observed between the experimental metal content and the theoretical value of 50%. However, the catalysts prepared by coprecipitation methods, CP and SACP, showed a metal content slightly lower than the theoretical value, which could be due to the formation of copper ammonium complexes, such as $[Cu\ (NH_3)_4]^{2+}$, preventing the complete precipitation of copper [51].

Table 1. Metal content, textural properties, and crystallite sizes of calcined/reduced CuAl catalysts.

Catalyst	Composition [a] (%)	S_{BET} [b] (m^2/g)	V_p [c] (cm^3/g)	d_p [c] (nm)	XRD D [d] (nm)
CuAl-AC1	50.5	43/31	0.06/0.09	3.2/9.9	21.0/21.6/27.7
CuAl-PP	52.2	63/100	0.17/0.24	4.7/6.2	28.4/23.1/35.4
CuAl-CP	47.4	144/153	0.32/0.39	8.0/8.0	14.9/-/22.3
CuAl-SACP	48.2	69/78	0.24/0.27	3.7/3.3	24.7/-/32.8

[a] Calculated as Cu/(Cu + Al) (mol/mol). [b] BET method. [c] BJH adsorption branch. [d] $CuO/CuAl_2O_4/Cu^0$ crystal size calculated from Scherrer's equation of calcined and reduced (Cu^0) catalysts.

The results of N_2 adsorption measurements are also shown in Table 1. The S_{BET} (m^2/g) of the calcined catalysts followed the order CuAl-CP (144) > CuAl-SACP (69) > CuAl-PP (63) > CuAl-AC1 (43). The V_p (cm^3/g) values presented the same sequence order: 0.32 > 0.24 > 0.17 > 0.06. The highest pore diameter (d_p, nm) was reached by CuAl-CP (8.0), followed by CuAl-PP (4.7), CuAl-SACP (3.7), and CuAl-AC1 (3.2). The N_2 adsorption–desorption isotherms of the calcined are shown in Figure 1a, while Figure 1b shows the pore distribution. All the calcined CuAl catalysts exhibit a Type IV isotherm, which is associated with mesoporous materials due to hysteresis. The CuAl-PP and CuAl-CP catalysts show a pore size distribution centered at 4.7 and 8 nm, respectively, while the CuAl-SACP and CuAl-AC1 catalysts show a broader pore size distribution.

The results of Table 1 show the influence of the preparation method on the textural properties of calcined catalysts. The catalysts prepared by PP and AC methods, which include a combustion stage, showed lower values of S_{BET} and V_P than those prepared by coprecipitation, CP and SACP. Thus, the methods that imply a combustion step, PP and AC, tend to obtain less porous materials due to sintering and agglomeration phenomena. Often, materials prepared by a coprecipitation method exhibit a higher pore diameter value than those prepared by other methods such as PP [34]. This is clearly observed when comparing CuAl-PP and CuAl-CP catalysts. The use of CTAB as a structure-directing agent in the literature has shown opposite tendencies in S_{BET} and pore size compared to preparations without CTAB [40,42]. This has exposed the relevance of the CTAB/metal ratio. Kang et al. [42] concluded that SACP materials with a CTAB/metal ratio higher than the

optimized value tend to show a lower specific surface area due to CTAB's decomposition. CTAB's decomposition produces gases and heat which can destroy the pore walls of the catalysts and increase the pore diameter. In this work, the CuAl-SACP catalyst (Figure 1b) shows large-diameter pores.

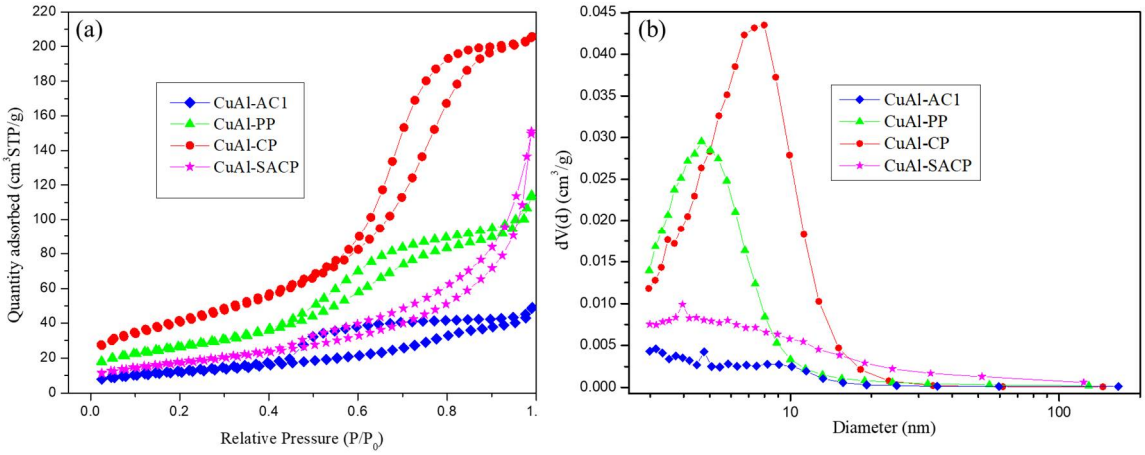

Figure 1. N_2 adsorption–desorption isotherms (**a**). Pore size distribution of adsorption branch (**b**) of the calcined CuAl catalysts. Calcination temperature: 650 °C.

The effect of the reduction step on the textural properties of the catalysts is mainly centered on an increase of the specific surface area, with the exception of the catalyst with the lowest BET surface area of all, the CuAl-AC1, in which instead of increasing it decreases; the other feature to highlight is that the rise for the rest of the catalysts is more noticeable in the polymeric precursor, CuAl-PP. The pore volume increases regularly in all catalysts once they are reduced, while the pore diameter depends on the preparation method.

Table 2 shows the textural properties of the used CuAl catalysts in the liquid and gas phases. Figure 2a,b presents the N_2 adsorption–desorption isotherms for the used catalysts in the liquid phase and gas phase, respectively.

Table 2. Textural properties, crystallite sizes, and carbon content of CuAl catalysts used in liquid/gas phase.

Catalyst	S_{BET} [a] (m^2/g)	V_p [b] (cm^3/g)	d_p (nm)	XRD D [c] (nm)	Carbon Content (Gas Phase) [d]
CuAl-AC1	51/45	0.13/0.11	3.2/6.0	38.8/31.2	15.46
CuAl-PP	37/87	0.10/0.20	3.5/7.4	31.3/36.2	27.17
CuAl-CP	53/141	0.15/0.33	3.7/8.9	24.7/25.8	31.75
CuAl-SACP	65/69	0.23/0.28	3.1/5.0	20.0/33.6	15.54

[a] BET method. [b] BJH adsorption branch. [c] Cu_2O/Cu^0 crystallite size calculated from Scherrer's equation of the used samples in liquid/gas phase. [d] Calculated as mg C/($g_{cat} \cdot g_{Reacted\ glycerol}$).

After the use of CuAl catalysts in the liquid phase (PRL), most of the catalysts changed their textural properties. Although all catalysts presented a Type IV isotherm (Figure 2a), most of the catalysts changed their hysteresis loop compared to the calcined catalysts. The modification of the textural properties after being in the liquid phase is influenced by the catalyst preparation method. Thus, the CuAl-SACP catalyst showed a high stability, with similar values of S_{BET} and V_P compared to the calcined catalyst. The CuAl-PP and CuAl-CP catalysts decreased the S_{BET} significantly, with values of 41% and 63%, respectively, compared to the calcined catalyst. The V_P and d_p values of these catalysts also decreased, while the S_{BET} and V_P values of the CuAl-AC1 catalyst showed a slight increase. The

S_{BET} (m^2/g) of the catalysts used in the liquid phase followed the order CuAl-SACP (65) > CuAl-CP (53) > CuAl-AC1 (51) > CuAl-PP (37).

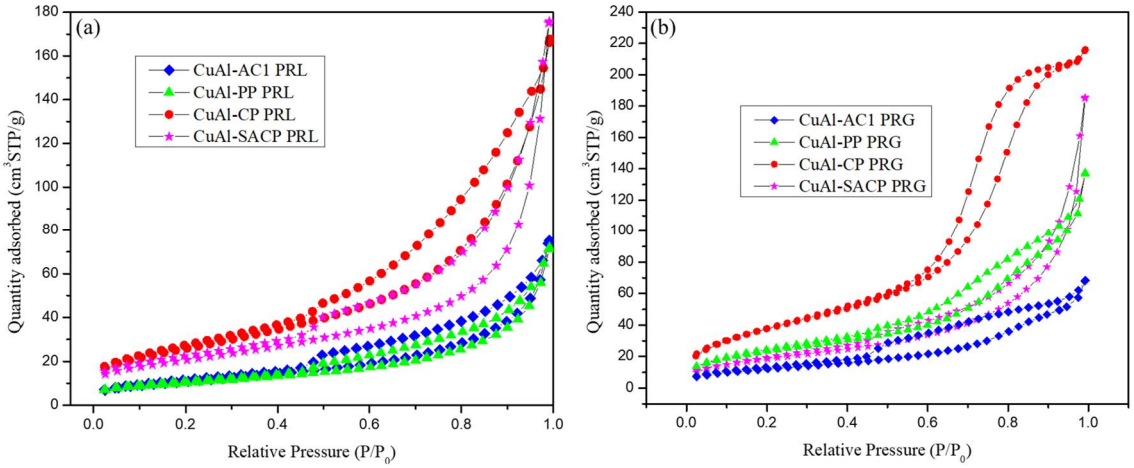

Figure 2. N_2 adsorption–desorption isotherms of used CuAl catalyst (**a**) in liquid phase and (**b**) in gas phase. Liquid-phase reaction conditions: 227 °C, 34 bar, 10 wt% glycerol, and 10 g cat min/g gly. Gas-phase reaction conditions: 227 °C, 1 bar, 10 wt% glycerol, and 30 g cat min/g gly.

After the use of CuAl catalysts in the gas phase, the N_2 adsorption–desorption isotherms (Figure 2b) were almost unmodified compared to the calcined catalysts. The S_{BET}, V_P, and d_p values were similar to those of the reduced catalysts, showing a small decrease in S_{BET} and V_P in most of the catalysts.

The S_{BET} value (m^2/g) of the catalysts used in the gas phase (PRG) showed the following tendency: CuAl-CP (141) > CuAl-PP (87) > CuAl-SACP (69) > CuAl-AC1 (45).

These results indicate that the operating conditions in the liquid phase with pressurized liquid water significantly decreased the textural properties of most of the catalysts, while the operating conditions in the gas phase barely had any influence. This fact was also reported by Lete et al. [24].

2.1.2. XRD Results

Figure 3a shows the XRD patterns of calcined CuAl catalysts synthesized by different preparation methods: CuAl-AC1, CuAl-PP, CuAl CP, and CuAl-SACP. The diffraction peaks at 32.6°, 35.6°, 38.8°, and 48.9° reveal the presence of a CuO phase (JCPDS file n°. 00-048-1548) [52], while peaks located at 31.1°, 37.0°, and 44.7° correspond to the $CuAl_2O_4$ spinel phase (JCPDS file n°. 01-078-1605) [53]. The presence of a CuO phase can be observed in all CuAl catalysts. However, the presence of the $CuAl_2O_4$ spinel phase is just elucidated in the CuAl-AC1 and CuAl-PP catalysts. The CuAl materials obtained through preparation methods which include a gelation–combustion step, CuAl-AC1 and CuAl-PP, have shown spinel-type phases ($CuAl_2O_4$) which implies a higher level of metal–support interaction, as can be seen in previous reports [47].

The crystallite sizes of the CuO and $CuAl_2O_4$ phases are shown in Table 1. The crystallite sizes (nm) of the CuO phase follow the tendency of CuAl-PP (28.4) > CuAl-SACP (24.7) > CuAl-AC1 (21.0) > CuAl-CP (14.9). On the other hand, the crystallite size of the $CuAl_2O_4$ phase (nm) is as follows: CuA-PP (23.1) > CuAl-AC1 (21.6).

These results evidence that the CuAl-CP catalyst displayed the lowest average crystallite size of the CuO phase, demonstrating the highest dispersion of this oxide. On the other hand, the CuAl-PP catalyst showed the highest value, which could be due to the combustion step in this synthesis that could promote particle sintering, reducing its dispersion. The preparation of the CuAl-AC1 catalyst showed a combustion stage of higher

intensity than the CuAl-PP catalyst. Despite this fact, the CuAl-AC1 catalyst showed a lower average crystallite size of CuO than the CuAl-PP catalyst. This may be due the higher metal–support interaction caused by the greater amount of Cu found in the spinel-like structure.

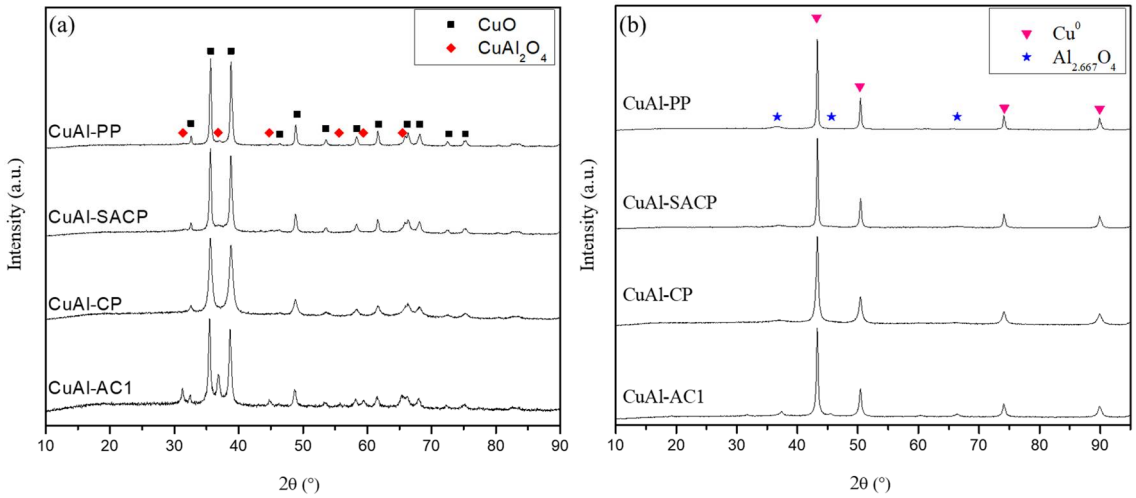

Figure 3. XRD patterns of CuAl catalysts, calcined (**a**) and reduced (**b**).

Figure 3b shows the XRD patterns of the reduced catalysts. It is observed that the reduction treatment completely reduces the CuO phases in all the catalysts to Cu^0. The Cu^0 phase can be elucidated by diffraction peaks at 2θ = 43.3°, 50.4°, 74.1°, and 89.9° (JCPDS n°. 01-085-1326) [24]. $Al_{2.667}O_4$ phases can be also elucidated by diffraction peaks at 2θ = 36.9°, 45.6°, and 66.4° (JCPDS n°. 01-080-1385) [24]. The $Al_{2.667}O_4$ phase has an Al/O ratio of 0.6675, which is higher than that obtained for the Al_2O_3 phase. This may be due to the presence of bridging oxygen in our catalysts' structure.

The crystallite size of the Cu^0 phase was also calculated using Scherrrer's equation. As Table 1 shows, the highest Cu^0 crystallite size of the activated catalysts was observed in CuAl-PP (35.4 nm), followed by CuAl-SACP (32.8 nm), CuAl-AC1 (27.7 nm), and CuAl-CP (22.3 nm). This is the same order as that of CuO in the calcined catalysts. However, there appears to be no correlation when comparing preparation methods involving a combustion stage (AC1 and PP) with those involving a precipitation stage (CP and SACP). It is important to highlight that the lowest value of the crystallite size was reached by the CuAl-CP catalyst, showing the beneficial effect of the coprecipitation step referred to metal dispersion.

Figure 4a shows the XRD patterns of the used catalysts in the liquid phase. The signals at 29.8°, 36.4°, 42.3°, 61.4°, and 73.6° reveal the presence of a Cu_2O phase (JCPDS n°. 00-005-0667) [54]. The presence of AlO(OH) can be also elucidated by peaks at 28.1°, 49.0°, and 55.2° (JCPDS n°. 00-021-1307) [55]. The Cu^0 phase can be also appreciated by peaks at 43.3°, 50.4°, 74.1°, and 89.9° (JCPDS n°. 01-085-1326). The presence of a Cu^0 phase, detected in all used catalysts, is a consequence of the catalyst activation treatment with a H_2 stream previous to the reaction.

The crystallite size of Cu_2O of the catalysts used in the liquid phase at 36.6° was calculated by Scherrer's equation and is shown in Table 2. The highest value was reached by CuAl-AC1 (38.8 nm), followed by CuAl-PP (31.3 nm), CuAl-CP (24.7 nm), and CuAl-SACP (20.0 nm).

The presence of Cu_2O phases in the used Cu catalysts is a common issue [27,56,57]. The presence of this phase may be due to a reversible reduction of the spinel phase or to the partial oxidation of Cu^0 to Cu^+ during the reaction. Khasin et al. [27,58,59] proposed

that Cu species conforming spinel phases showed a reversible reduction property, which could justify the existence of Cu_2O phases in our used catalysts prepared by AC1 and PP. Velasquez et al. [50] also showed the reversible reduction to Cu^+ from their $CuLa_2O_4$ catalysts under experimental conditions. Other works, such as Xiao et al. [27], have suggested the possible electron transfer from Cu^0 to chemisorbed acetol during glycerol hydrogenolysis, promoting its oxidation.

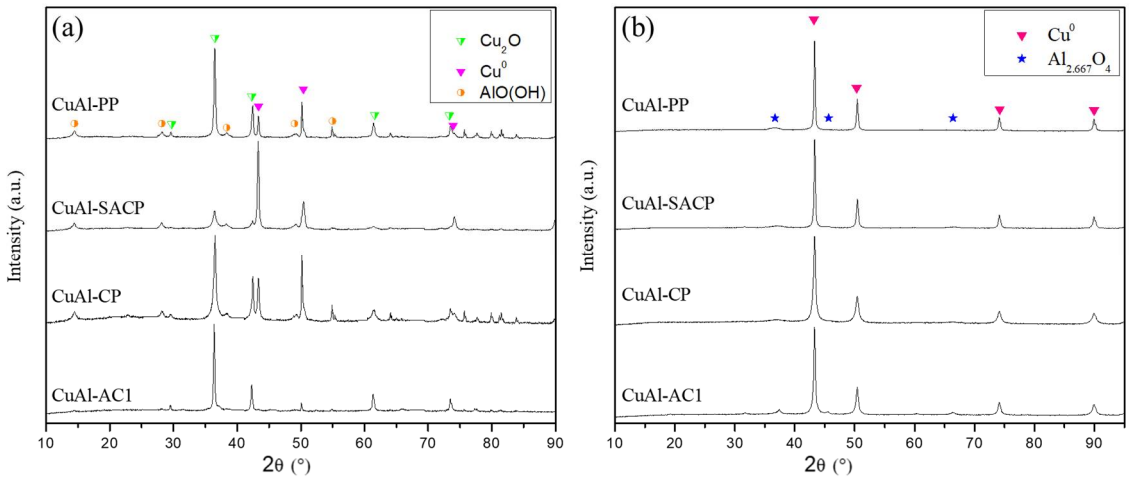

Figure 4. XRD patterns of used CuAl catalysts in the liquid phase (**a**) and in the gas phase (**b**). Liquid-phase reaction conditions: 227 °C, 34 bar, 10 wt% glycerol, and 10 g cat min/g gly. Gas-phase reaction conditions: 227 °C, 1 bar, 10 wt% glycerol, 30 g cat min/g gly.

Boehmite, AlO(OH), is another phase present in the used catalysts in liquid-phase reactions. The presence of this phase is due to the hydration of Al_2O_3 phases under reaction conditions and it may decrease the activity of the catalysts [60].

Figure 4b shows the XRD patterns of the CuAl catalysts used in the gas-phase reactions. The Cu^0 phase (JCPDS n°. 01-085-1326) [24] can be clearly identified in all used catalysts. The $Al_{2.667}O_4$ phase (JCPDS n°. 01-080-1385) [24] is slightly identified. The tendency of the Cu^0 average crystallite size of the reduced catalysts (nm), shown in Table 1, is as follows: CuAl-PP (35.4) > CuAl-SACP (32.8) > CuAl-AC1 (27.7) > CuAl-CP (22.3). A similar tendency of the Cu^0 average crystallite size (nm) of the used catalysts in the gas phase can be shown in Table 2, followed the order: CuAl-PP (36.2) > CuAl-SACP (33.6) > CuAl-AC1 (31.2) > CuAl-CP (25.8). A slight sintering effect can be elucidated in the gas phase, as previously reported [24].

In order to study the possible electronic transfer from Cu^0 to the substrate in the liquid phase, as proposed above, the CuAl-PP catalyst was analyzed by XRD after being subjected to an aqueous medium without glycerol. Figure 5 shows the XRD patterns after four stages: calcination, activation with H_2, aqueous medium at 227 °C and 34 bar, and use in glycerol conversion. It is clearly observed that the hydrothermal conditions strongly promote boehmite formation and the Cu^0 phase is almost unaffected. On the other hand, the used CuAl-PP catalyst clearly shows oxidation from Cu^0 to Cu_2O. The Cu^0 phase strongly decreases while Cu_2O phases sharply appear. These results are in concordance with those of other authors [27]. They suggested the electron transference from Cu^0 to chemisorbed acetol during glycerol hydrogenolysis. In this way, Cu may act as an electron transfer agent for acetol hydrogenation to 1,2-PDO in the liquid phase. In the gas phase (Figure 4b), this phenomenon cannot be elucidated, i.e., Cu^0 is not oxidized to Cu_2O during the reaction, as previous works established [24]. This fact can suggest the role of pressure in promoting the electron transference phenomenon.

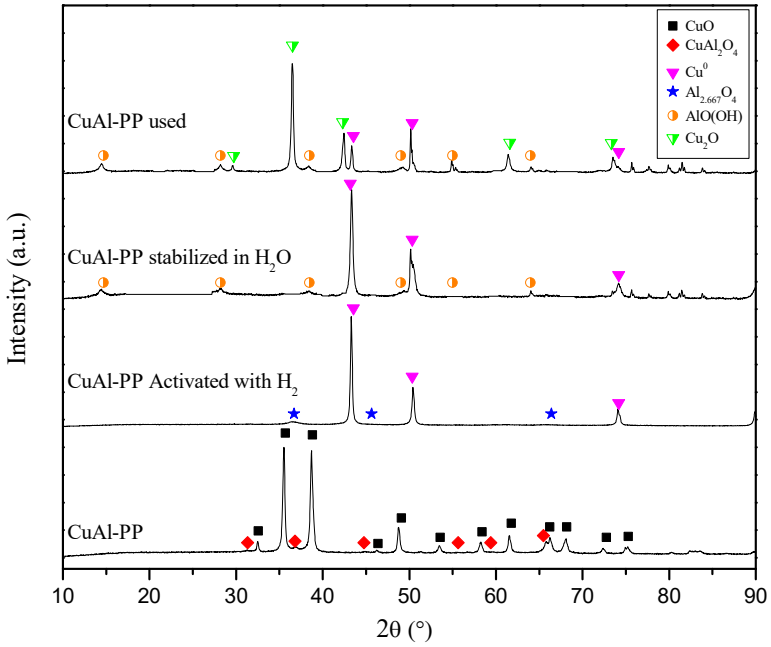

Figure 5. XRD patterns of different stages of CuAl-PP catalyst: calcined, reduced, stabilized in liquid H_2O, and used in liquid-phase reaction. Liquid-phase reaction conditions: 227 °C, 34 bar, 10 wt% glycerol, and 10 g cat min/g gly.

2.1.3. H_2 Temperature Programmed Reduction

The H_2-TPR profiles are displayed in Figure 6. All CuAl catalysts have reduction peaks between 185–257 °C, which can be roughly divided into two reductive phenomena: low-temperature peaks and high-temperature peaks, as was elucidated previously [61,62]. The low-temperature reduction peaks are attributed to the reduction of Cu^{2+} phases to Cu^0 in highly dispersed CuO with a small particle size, while the high-temperature reduction peaks are related to the reduction of CuO to Cu^0 with a larger particle size, as has been previously studied in other works [63–65].

The CuAl catalysts that exhibit spinel phases in XRD analysis (Figure 3a), such as CuAl-PP and CuAl-AC1, show additional reduction peaks that correspond to the reduction of the $CuAl_2O_4$ spinel phase between 326–359 °C, as previously reported [66]. The ratio of the different phases is displayed in Table 3.

Table 3. H_2-TPR results of the calcined CuAl catalysts.

	Temperature (°C)/Relative Amount (%) [a]		
Catalyst	**T1/F1**	**T2/F2**	**T3/F3**
CuAl-CP	231/75.8	257/24.2	-
CuAl-SACP	235/41.8	252/58.2	-
CuAl-AC1	185/11.9	228/76.0	355/12.1
CuAl-PP	228/77.5	250/20.5	359/2.0

[a] Calculated from Gaussian deconvolution from H_2-TPR profiles.

These results are consistent with those obtained using X-ray diffraction (XRD) and justify the presence of $CuAl_2O_4$ phases. The PP synthesis also has a characteristic spinel reduction peak but with a lower relative amount. This may be a consequence of the lower temperatures reached during the combustion step, characteristic for AC1 and PP synthesis, since spinel phases need high temperatures to be formed, as previously studied [67].

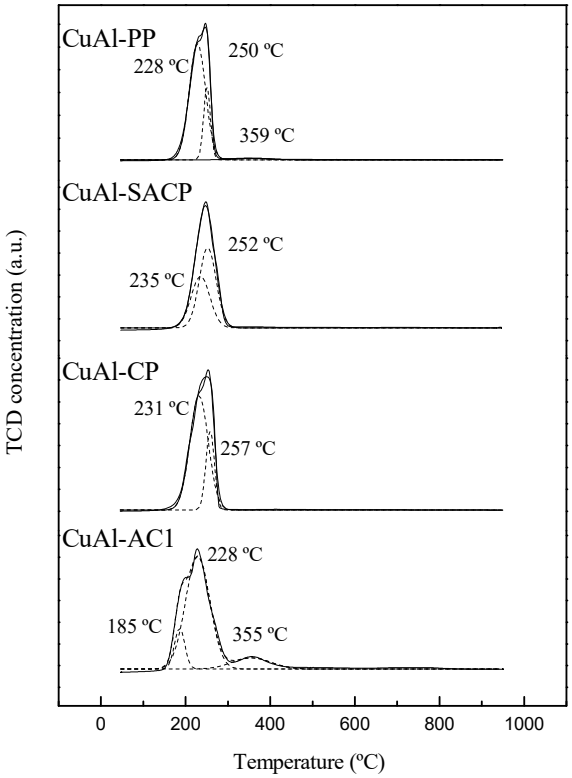

Figure 6. H_2-TPR profiles of calcined CuAl catalysts.

2.1.4. SEM-EDS Analysis and Textural Features

With the aim of studying the surface morphology of the calcined and used catalysts, field emission scanning electron microscopy (FESEM) was used. Figure 7 shows the FESEM images of the CuAl calcined catalysts.

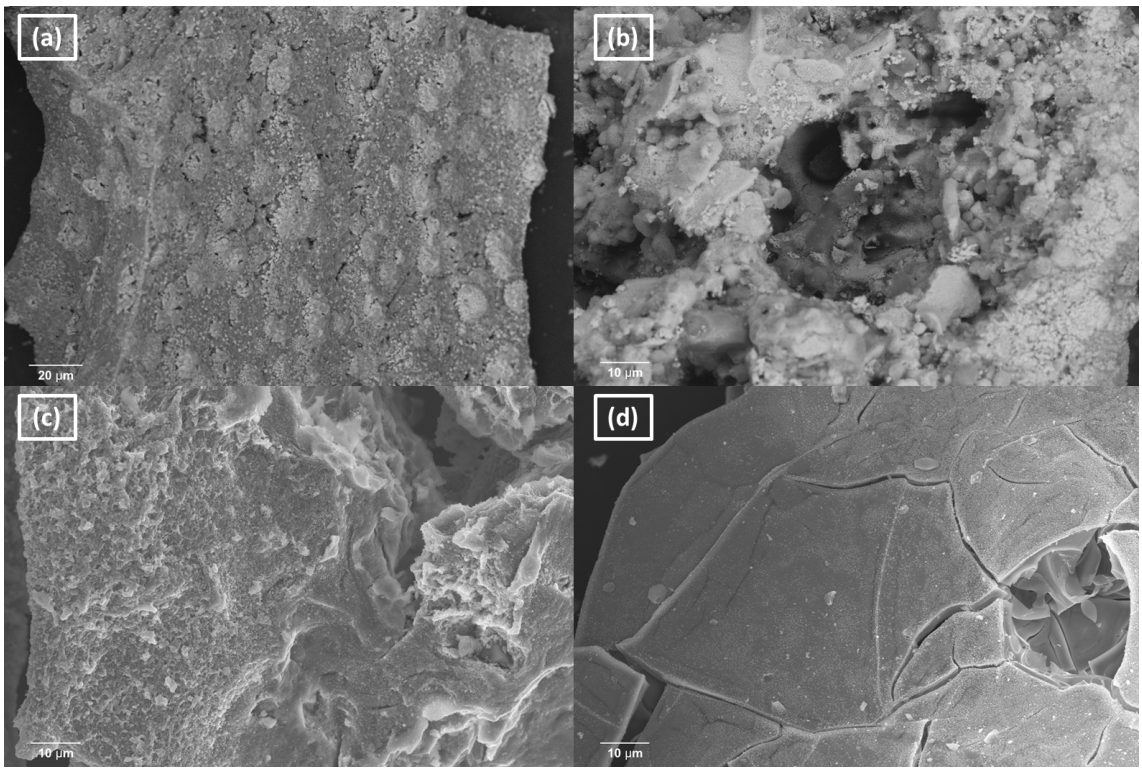

Figure 7. FESEM images of the calcined catalysts: CuAl-PP (**a**), CuAl-SACP (**b**), CuAl-CP (**c**), and CuAl-AC1 (**d**). Calcination temperature: 650 °C.

As can be seen in Figure 7, the CuAl catalysts prepared via a coprecipitation method, SACP and CP (Figure 7b and c respectively), tend to show higher surface roughness as well as a more noticeable dispersion of Cu across the catalyst's surface. This may explain their highest S_{BET} values of 144 and 69 m^2/g, respectively. On the other hand, CuAl-PP (Figure 7a) exhibits a lower surface roughness and Cu dispersion, and small spherical Cu domains on the surface can be slightly distinguished. The CuAl-AC1 catalyst (Figure 7d) shows a relatively smooth surface; this may explain its low S_{BET} of 43 m^2/g (Table 1). These results clarify the notable influence that the preparation method has on the properties of CuAl catalysts.

Figure 8 shows the effect of the severe liquid-phase reaction conditions on the catalysts. The appearance of Cu^0 structures can be observed on the surface of the catalyst due to the reduction treatment. Flower-like particles, elongated shapes, and thick plate structures can be also elucidated in all the used catalysts in the liquid phase. These structures are related to the formation of boehmite phases due to the hydrothermal reaction conditions [68,69]. These results are in concordance with the XRD measurements (Figure 4a).

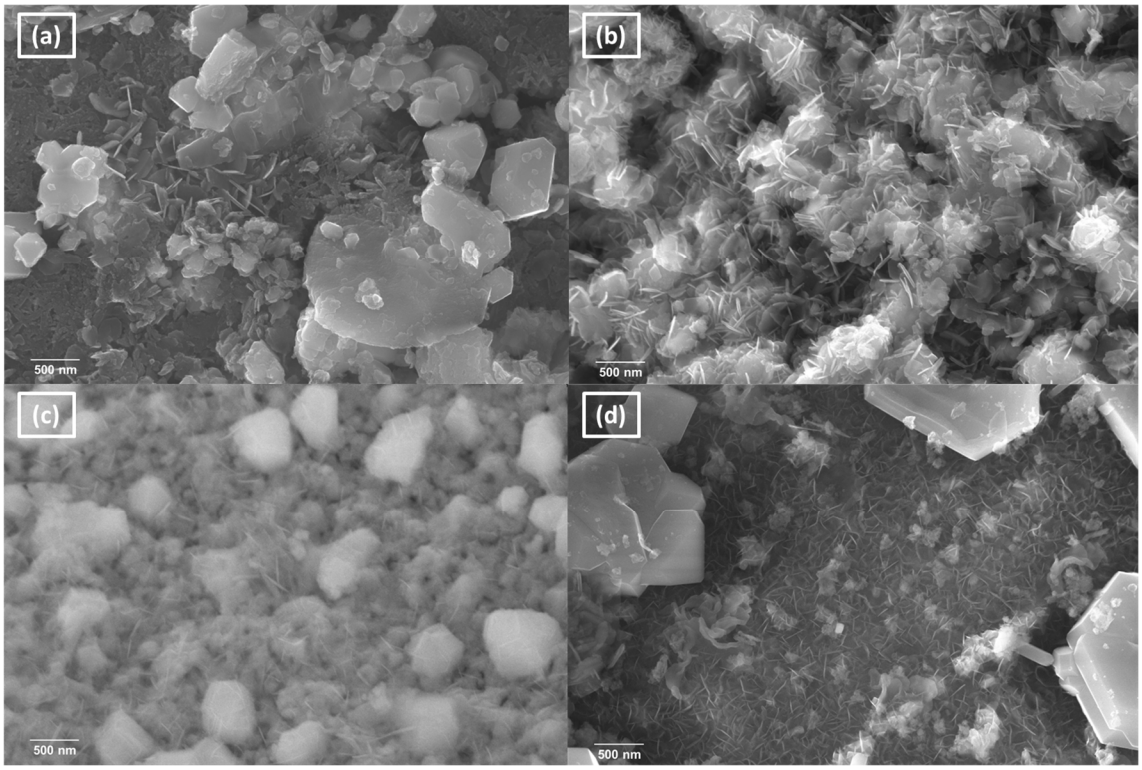

Figure 8. FESEM images of used catalysts in liquid phase: CuAl-PP (**a**), CuAl-SACP (**b**), CuAl-CP (**c**), and CuAl-AC1 (**d**). Liquid-phase reaction conditions: 227 °C, 34 bar, 10 wt% glycerol, and 10 g cat min/g gly.

Figure 8 clearly shows the impact of the preparation method in the properties of the used catalysts in the liquid phase. The CuAl-PP and CuAl-AC1 catalysts (Figure 8a and d, respectively) showed higher particle sizes than the CuAl-SACP and CuAl-CP catalysts (Figure 8b and c respectively), especially the brighter structures, which may correspond to Cu^0. These results are in concordance with the calculated average crystallite size of the used catalysts in the liquid phase (Table 2).

2.1.5. Leaching Studies and Carbon Content in Used Catalysts

The liquid products were analyzed by ICP-OES with the objective of determining the leaching of metals from the catalysts during the liquid-phase reaction. Figure 9 shows the metal mass percentage leaching from the content in fresh catalysts determined by ICP-OES.

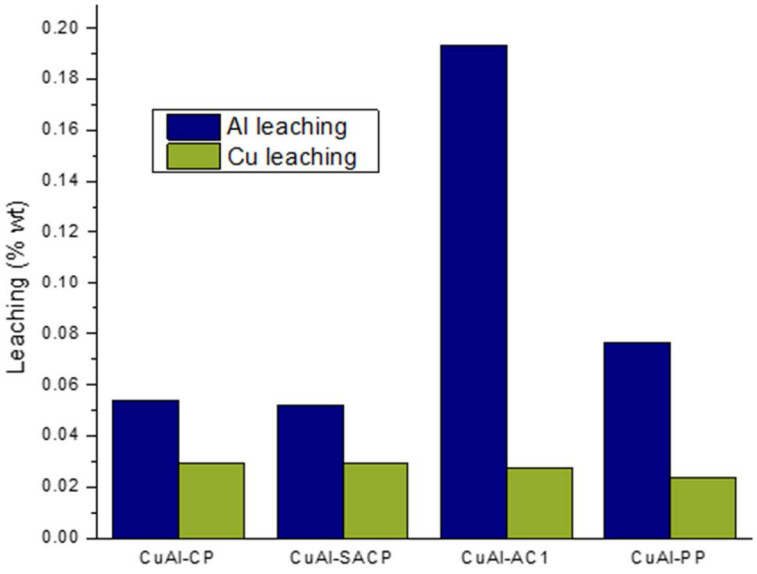

Figure 9. Mass percentage of Cu and Al leaching of the used catalysts in liquid phase. Liquid-phase reaction conditions: 227 °C, 34 bar, 10 wt% glycerol, and 10 g cat min/g gly.

It is observed that Al leaching is greater than Cu leaching in all catalysts. The CuAl-AC1 catalysts show the highest Al leaching (0.193%), significantly higher than the rest of the catalysts, with Al leaching less than 0.08%. Cu leaching is smaller than 0.03% for all catalysts. The CuAl-CP catalyst shows leaching values similar to those obtained with the coprecipitated CuAl catalyst of Lete et al. [24]. Cu leaching was very similar in both the present study and Lete's article. However, Lete's catalyst showed greater Al leaching than this study, which could be due to the higher Al content.

The carbon content of the used catalysts was studied by elemental analysis. The carbon content on the catalysts used in the liquid phase was undetectable or below the detection limit, while the catalysts used in the gas phase showed detectable carbon deposition values (Table 2). The carbon content, expressed as mg C/(g catalyst g reacted glycerol), followed the order CuAl-CP (31.75) > CuAl-PP (27.17) > CuAl-SACP (15.54) ≈ CuAl-AC1 (15.46).

There could be some reasons to explain the low carbon formation after the reaction in the gas phase, such as the Cu°-Al_2O_3 assembly in the CuAl-SACP catalyst or the presence of $CuAl_2O_4$ spinel in the CuAl-AC1 catalyst. It was clearly observed that these catalysts, CuAl-AC1 and CuAl-SACP, with low carbon formation showed low 1,2-PDO selectivity. Then, in the reaction mechanism, acetol could be desorbed easily from the active site, which hindered acetol conversion to 1,2-PDO and carbon formation. Chiu et al. proposed that in the dehydration of glycerol to acetol the scavenging of hydrogen from the glycerol generates 1,2-PDO and undesired products, including a solid residue [38]. This residue could be the formation of carbon.

2.1.6. TGA Measurements

Figure 10 shows the TGA results obtained from the CuAl catalyst used in the liquid phase. Step I, between 25–140 °C, is associated with the loss of physisorbed water, while Step II, between 140–700 °C, is associated with the dehydration of boehmite to Al_2O_3. Thus, a greater weight loss is due to a greater formation of boehmite during the reaction

conditions. The % weight loss in Step II follows the following trend: CuA-SACP (8.78%) > CuAl-CP (6.07%) > CuAl-AC1 (4.89%) > CuAl-PP (4.36%). These results indicate that CuAl catalysts obtained by precipitation methods (CP and SACP) tend to form larger amounts of boehmite under the selected reaction conditions.

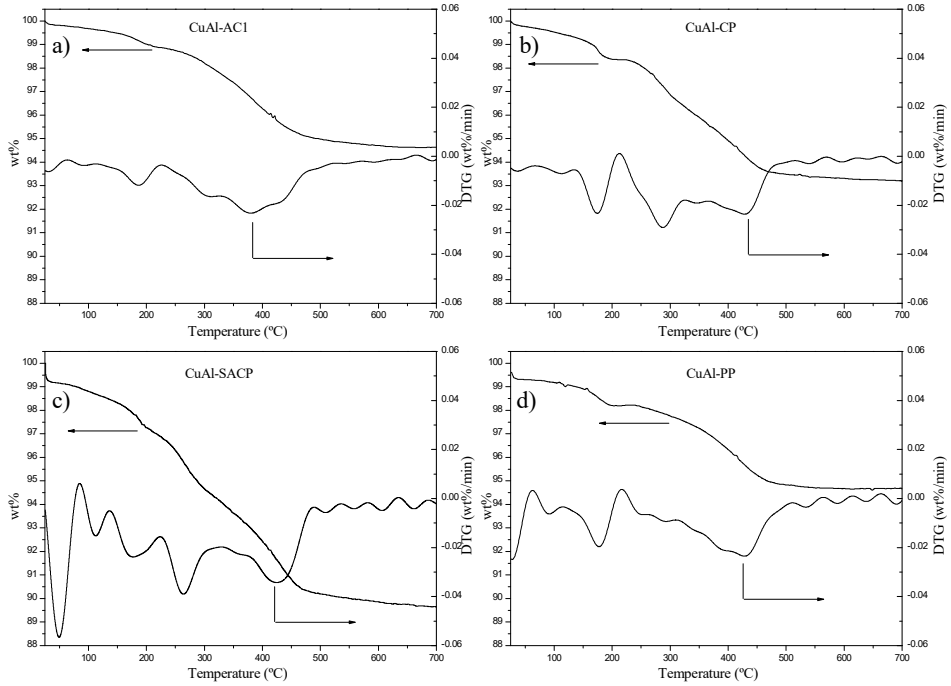

Figure 10. TGA/DTG curves of the used CuAl catalysts in liquid phase: CuAl-AC1 (**a**), CuAl-CP (**b**), CuAl-SACP (**c**), and CuAl-PP (**d**). Liquid-phase reaction conditions: 227 °C, 34 bar, 10 wt% glycerol, and 10 g cat min/g gly.

There could be a relationship between the formation of the spinel phase, present in CuAl catalysts prepared by AC1 and PP, and the lower formation of boehmite. The existence of the boehmite phase in the CuAl catalyst is not related to the increase in Al leaching. The CuAl-AC1 and CuAl-PP catalysts showed a slightly lower Al content than the rest of catalysts (Table 1), as well as a slightly higher level of Al leaching, and are catalysts with low boehmite formation. This may suggest that the formation of boehmite could prevent the leaching of Al.

2.1.7. XPS Analysis

XPS was used to assess the composition and oxidation state of Cu on the surface of the catalysts used in liquid-phase reactions. XPS data from Cu 2p, Al 2p, and Cu LMM are presented in Figure 11a, b and c, respectively.

The deconvolution of the Cu 2p signal into five contributions is shown in Figure 11a. The contribution of the satellite peaks, intermediate signals, was subtracted. The deconvolution of Cu 2p ½ and 3/2 into two signals confirms the presence of different oxidation states of Cu. The Cu $2p_{3/2}$ signal can be deconvoluted into two contributions: at 934.0 eV (referred to Cu^{2+}) and 933.0 eV (referred to Cu^0/Cu^+) [70,71]. Furthermore, an intermediate signal (satellite peak) at 943.5 eV also confirms the presence of Cu^{2+} phases on the surface of the catalysts used, as can be seen in previous reports [27,72]. However, in the Cu 2p signal it is not possible to distinguish between Cu^0 and Cu^+. Figure 11b shows that the Al 2p peak can be assigned to the oxidation state of Al^{3+}, which corresponds to the oxidized phases of Al on the surface [73], also clarified by the XRD data (Figure 4a). The Al 2p peak is subtracted from the deconvoluted signal by removing the Cu 3p contribution.

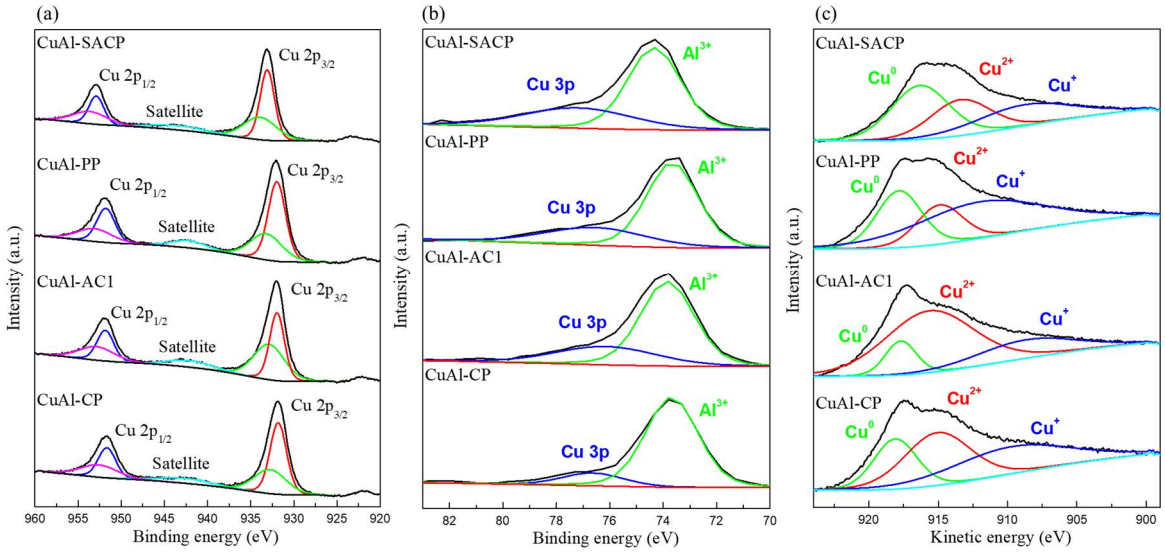

Figure 11. X-ray photoelectric high-resolution spectra for the catalysts used in liquid phase: (**a**) Cu 2p; (**b**) Al 2p; (**c**) Cu LMM. Liquid-phase reaction conditions: 227 °C, 34 bar, 10 wt% glycerol, and 10 g cat min/g gly.

The Cu LMM signal allows to distinguish the three oxidation states of Cu. The patterns obtained from the samples used are shown in Figure 11c. The XAES spectra obtained corroborate the presence of the three oxidation states of Cu.

The results in Table 4 show that the highest Cu/Al ratio was achieved with CuAl-PP (1.18), followed by CuAl-SACP (0.15) > CuAl-AC1 (0.13) > CuAl-CP (0.11). These results show the notable influence of the preparation method on the properties of the catalysts, as well as on the catalysts used. It is clear that the Cu content of CuAl-PP is much higher than that of the other catalysts used. In this case, the sintering and gelation phenomena, derived from the preparation method, seem to contribute to maintaining a higher Cu content on the surface. The other three catalysts have a very similar value, indicating that the gelation step of the PP preparation method is key to fixing a higher Cu content on the surface.

Table 4. XPS surface analysis of the used catalysts in liquid phase.

Used Catalysts	Cu^0 (%) [a]	Cu^+ (%) [a]	Cu^{2+} (%) [a]	Cu/Al Ratio [b]
CuAl-SACP	42.4	28.0	29.5	0.15
CuAl-PP	23.8	46.1	30.2	1.18
CuAl-AC1	12.6	21.9	65.5	0.13
CuAl-CP	24.3	36.5	39.2	0.11

[a] Data obtained from Cu LMM analysis. [b] Data obtained from Cu 2p and Al 2p analysis.

The percentages of the Cu oxidation state of the catalysts used are also shown in Table 4. The Cu^0 (%) follows the following trend: CuAl-SACP (42.4) > CuAl-CP (24.3) > CuAl-PP (23.8) > CuAl-AC1 (12.6). Cu^+ follows a different trend: CuAl-PP (46.1) > CuAl-CP (36.5) > CuAl-SACP (28.0) > CuAl-AC1 (21.9). The highest value of Cu^{2+} (%) on the surface is achieved by CuAl-AC1 (65.5), followed by CuAl-CP (39.2) > CuAl-PP (30.2) > CuAl-SACP (29.5).

It is clear that the two methods that involve a precipitation step (CP and SACP) prevent the oxidation of Cu^0 during the liquid-phase reactions. This agrees with our XRD and TPR results. In this way, the presence of spinel phases seems to promote the reoxidation of Cu^0 in the liquid phase, as mentioned above. On the other hand, CuAl-PP seems to have a strong tendency to stabilize the Cu^+ phases. Thus, the greater metal–support interaction

may act to stabilize the Cu^{+}. However, the highest value of Cu^{2+} (%) is achieved by CuAl-AC1. This oxidation state appears to be extremely stable using this preparation method. As mentioned above, the $CuAl_2O_4$ spinel phases exhibit the tendency to promote the reverse oxidation of Cu^0. This is consistent with our XPS results. It is clear that the CuAl catalysts with the most intense spinel signal (Figure 3a) are those with the highest Cu^{2+} content after the reaction. Thus, it is important to choose the correct preparation method to control the presence of relative amounts of spinel phases. These relative amounts of spinel phases in the calcined catalysts can influence the reverse oxidation of Cu during the liquid-phase reaction, affecting the catalyst performance and the selectivity towards the liquid products obtained.

The above results clearly show the oxidation of CuAl catalysts during the liquid-phase experiments. Some modifications can be made to prevent or control Cu oxidation during liquid-phase reactions. Yao et al. [74] demonstrated that Ni can act to prevent Cu from being oxidized through a spillover effect. In this way, Ni can act by dissociating the H_2 produced and reducing the oxidized Cu during the liquid-phase reaction.

2.2. Catalytic Activity in the Liquid Phase

2.2.1. Influence of the Preparation Method

Figure 12a,b shows the experimental results using the CuAl catalysts in the liquid phase with a W/m ratio of 10 $g_{catalyst} \cdot min \cdot g_{glycerol}{}^{-1}$ (g cat min gly^{-1}). The carbon yield to liquids was higher than the carbon yield to gases for all catalysts. The carbon yields to products were very low, with the carbon yield to liquids being less than 4%. The CuAl-AC1 and CuAl-CP catalysts showed carbon yield to liquids values around 3.9%. The carbon yield to liquids obtained with the CuAl-SACP catalysts was around 2.4%, while that generated with CuAl-PP was 2.1%, the lowest value (Figure 12a). The carbon yield to gases was around 0.14% for the CuAl-AC1, CuAl-CP, and CuAl-SACP catalysts, while the CuAl-PP catalyst showed the lowest carbon yield to gases at 0.06%.

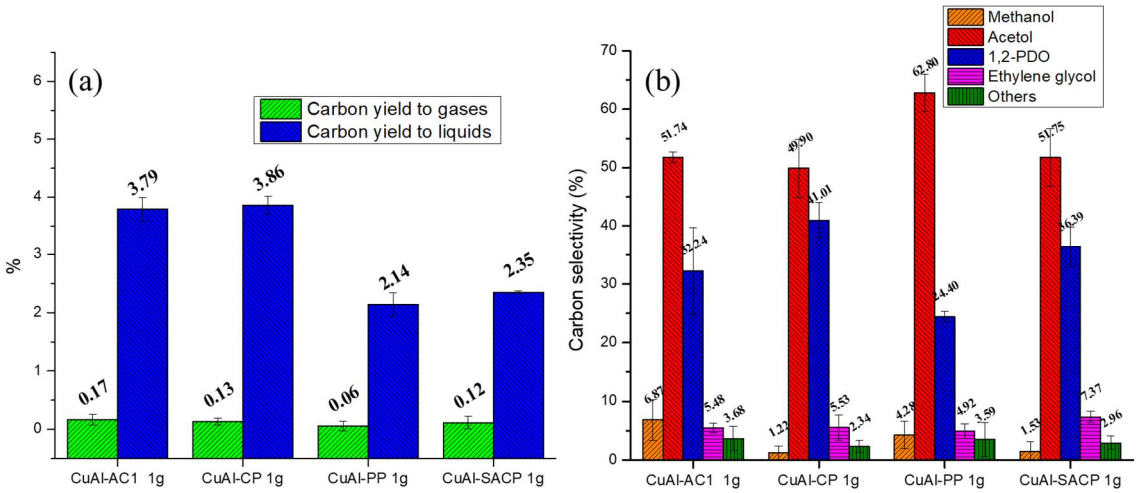

Figure 12. Catalytic performance of CuAl catalysts in the liquid phase. Carbon yield to products (**a**). Carbon selectivity to liquid products (**b**). Conditions: 227 °C, 34 bar, 10 wt% glycerol, and g cat min gly^{-1}.

Figure 12b shows the carbon selectivity to liquid products. Acetol and 1,2-PDO were the main products, showing in all cases a carbon selectivity for both products greater than 85%. The CuAl-AC1, CuA-CP, and CuAl-SACP catalysts showed similar values of carbon selectivities to acetol and 1,2-PDO, with values around 51% and 39% respectively. The CuAl-PP catalyst showed the highest values of carbon selectivity to acetol, with a

value around 63%, while the carbon selectivity to 1,2-PDO was around 24%. Other liquid products were ethylene glycol, and methanol. Minor amounts of acetaldehyde, acetone, methanol, isopropanol, ethanol, and acetic acid were also detected. To measure the real activity of the catalysts, experiments were carried out with inert sand. The results revealed carbon yield values of less than 0.5% in the products. The carbon selectivity to acetol and 1,2-PDO was 10.79% and 65.08%, respectively.

The carbon yield to liquids and gases, the effective activity, followed the order CuAl-CP ≈ CuAl-AC1 > CuAl-SACP > CuAl-PP. These results could be due to the size of the Cu crystallites' size after reduction (Table 1). The CuAl-CP catalyst had a Cu crystallite size, determined by Scherrer's equation, of 22.3 nm, a consequence of the high S_{BET} value in the calcined catalyst, 144 m^2/g. However, the S_{BET} of this catalyst decreased significantly to 53 m^2/g after being used in the liquid phase. The CuAl-AC1 catalyst showed a Cu crystallite size after reduction of 27.7 nm. The S_{BET} of this calcined catalyst and after its use in the liquid phase presented similar values, 43 and 51 m^2/g, respectively. The CuAl-SACP catalyst presented a Cu crystallite size after reduction of 32.8 nm. Furthermore, this catalyst showed significant stability in S_{BET} after its use in the liquid phase, with values of 69 and 65 m^2/g for the calcined and spent catalyst, respectively. The CuAl-PP catalyst showed the largest Cu crystallite size after reduction with a value of 35.4 nm. The S_{BET} of this catalyst was not stable after use in the liquid phase, 63 and 37 m^2/g were the S_{BET} values after calcination and use, respectively.

All these catalysts were modified after being used in the liquid phase, which was observed in XRD patterns with the presence of Cu_2O and boehmite phases. As can be observed in Figure 5 for the CuAl-PP catalyst, boehmite is generated from contact with liquid water at a temperature and pressure of 227 °C and 34 bar, respectively, during stabilization to reach the operating conditions prior to the glycerol reaction. On the other hand, the Cu_2O phase appeared after glycerol reaction.

Boehmite formation was estimated from TGA analysis (Figure 10). There appeared to be a relationship between boehmite formation and catalyst activity. Thus, the CuAl-PP and CuAl-AC1 catalysts showed low boehmite formation and their activity is very different.

The analysis of S_{BET} and V_p of the catalysts after use in the liquid phase did not show a clear trend with the catalyst activity. The CuAl-PP catalyst showed the lowest activity and this catalyst presented the lowest S_{BET} (37 m^2/g) and the lowest V_p (0.11 cm^3/g). However, the CuAl-SACP catalyst showed the highest S_{BET} (65 m^2/g) and the highest V_p (0.24 cm^3/g) and its activity was not the highest.

To explain the activity of the catalyst, two hypotheses have been found in the literature. The first hypothesis supports that these materials only have Cu^0 as the active phase, where H_2 is activated and glycerol is adsorbed through the hydroxyl group and cleaved [17]. Rasika et al. [15] elucidated the importance of the Cu^0 phase for the activation of glycerol, showing a drop in the conversion of glycerol using their catalysts without a prior activation treatment with H_2. The second hypothesis suggests that Cu catalysts have two different active sites: Cu^0, where H_2 is activated, and Cu^+, where the adsorption and cleavage of hydroxyl groups take place [38]. Furthermore, the influence of the Cu^0/Cu^+ ratio on the selectivity of the Cu catalysts has been suggested [15].

From the XPS results, Figure 13a has been prepared, which shows a relationship between the carbon yield to products and the Cu^0/Cu^+ ratio. The Cu^0/Cu^+ ratio around 0.6–0.7 showed the best catalytic activity. Xiao et al. [27] previously tested the synergetic effect of an optimal Cu^0/Cu^+ ratio, for which they obtained a maximum glycerol conversion value. Unlike our case, instead of modifying the preparation methods used, they modified the calcination and reduction temperature used. Their results show an optimal value of

the Cu^0/Cu^+ ratio of 6.6, different from ours (0.58–0.67). This may be due to the different composition of their catalysts, Cu-Cr.

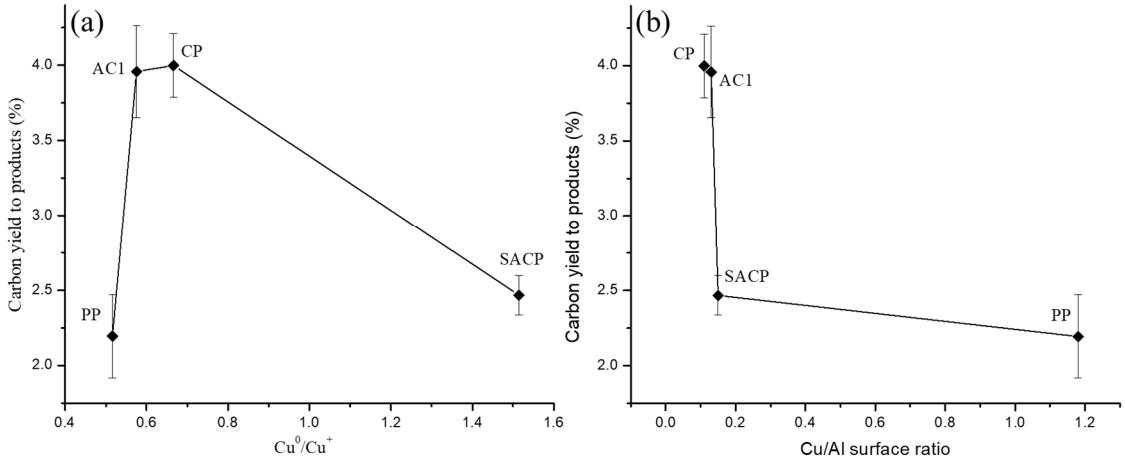

Figure 13. Correlation between surface Cu^0/Cu^+ ratio (**a**) or surface Cu/Al ratio (**b**) and carbon yield to products.

On the other hand, the Cu/Al surface ratio, also obtained from the XPS analysis, is shown in Figure 13b. These results clearly indicate that high concentrations of Cu on the surface of the catalysts negatively affect their activity. Therefore, we tentatively propose that there may be an optimal Cu/Al surface ratio that promotes Cu activity.

The CuAl-PP catalyst showed the lowest carbon yield to gases and the lowest carbon selectivity to EG. This may indicate that the acetol hydrogenation reaction is not favored, resulting in the highest acetol selectivity among all CuAl catalysts tested. On the other hand, EG production is commonly associated with H_2 production, as proposed in Figure 14 [75]. This lower H_2 production could also reduce the hydrogenation of acetol to 1,2-PDO.

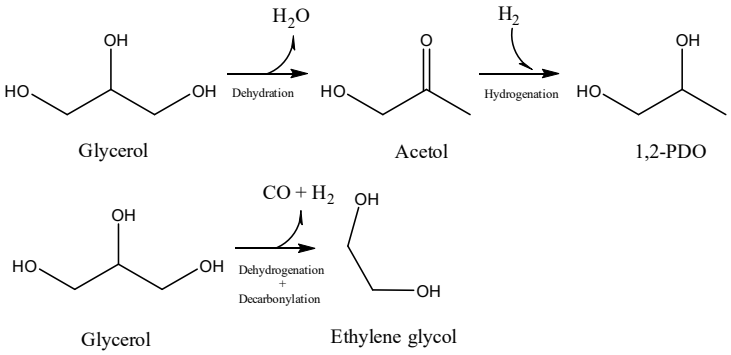

Figure 14. Reaction pathways of production of acetol, 1,2-PDO, and EG from glycerol.

2.2.2. Influence of the Catalyst Amount

Due to the low catalyst activity in the liquid phase using a W/m ratio of 10 g cat min gly^{-1}, a larger amount of catlayst was used, resulting in a W/m ratio of 30 g cat min gly^{-1}. For this, two preparation methods were selected: CuAl-PP, due to its high carbon selectivity to acetol, and CuAl-CP, due to its high carbon yield to liquids. CuAl-AC1 is also an interesting catalyst, but its low density was not appropriate. Figure 15a,b shows the experimental results.

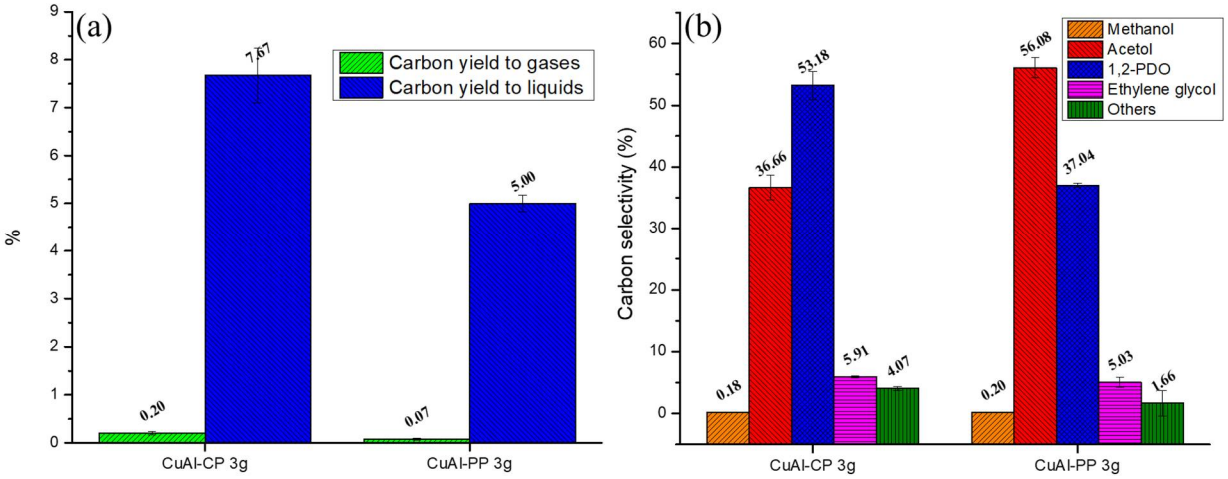

Figure 15. Catalytic performance of CuAl-CP and CuAl-PP catalysts in the liquid phase. Carbon yield to products (**a**). Carbon selectivity to liquid products (**b**). Conditions: 227 °C, 34 bar, 10 wt% glycerol, 30 g cat min gly^{-1}.

The increase in the amount of catalyst, as a consequence of the W/m ratio, caused an increase in the carbon yields to liquids and gases. For example, the carbon yield to liquids with the CuAl-CP catalyst was 3.9 and 7.7% for W/m ratios of 10 and 30 g cat min gly^{-1}, respectively. The trend observed using a W/m ratio of 10 $g_{catalyst}$·min·$g_{glycerol}{}^{-1}$, which indicated higher activity of the CuAl-CP catalyst than the CuAl-PP catalyst, is also followed using the ratio of 30 g cat min gly^{-1}. The carbon selectivity to liquid products (Figure 15b) was significantly modified with the increase of the W/m ratio of 30 $g_{catalyst}$·min·$g_{glycerol}{}^{-1}$. The main liquid product obtained using the CuAl-CP catalyst was 1,2-PDO. When the CuAl-PP catalyst was used, the main liquid product obtained was acetol, but the carbon selectivity to acetol was 56.1%, significantly lower than the value of 62.8% obtained with the W/m ratio af 10 g cat min gly^{-1}.

It is clear that an increase in the amount of catalyst leads to a lower carbon selectivity to acetol while increasing the carbon selectivity to 1,2-PDO. Based on our results, it can be seen that, regardless of the amount of catalyst, an increase in effective activity, quantified as total carbon yield, leads to higher carbon selectivity to 1,2-PDO and lower carbon selectivity to acetol. This trend was also observed in previous studies [76]. This suggests that the selectivity to these products is not only influenced by the catalyst used and its microstructure but also by the kinetic and thermodynamic influence inherent to the process itself. Studies, such as that of Yfanti et al. [77], have concluded that the kinetics of the combined reaction cycle followed a Langmuir–Hinshelwood reaction model with competitive adsorption processes between the reactant (glycerol) and reaction products (acetol). In this way, acetol can act by blocking the active centers, inhibiting the adsorption of glycerol. The hydrogenation of acetol to 1,2-PDO should promote its desorption, allowing greater glycerol activation processes.

2.3. Catalytic Activity in the Gas Phase

All CuAl catalysts were also studied in the gas phase at 227 °C and atmospheric pressure. As can be seen in Figure 16a, the highest carbon yield to liquid products is achieved by CuAl-SACP (59.38%), followed by CuAl-AC1 (49.00%), CuAl-CP (46.21%), and CuAl-PP (42.13%). The carbon yield to gaseous products is still very low and is very similar for three of the catalysts: CuAl-CP (0.68%), CuAl-AC1 (0.68%), and CuAl-SACP (0.65%). The lowest value is obtained from CuAl-PP (0.27%).

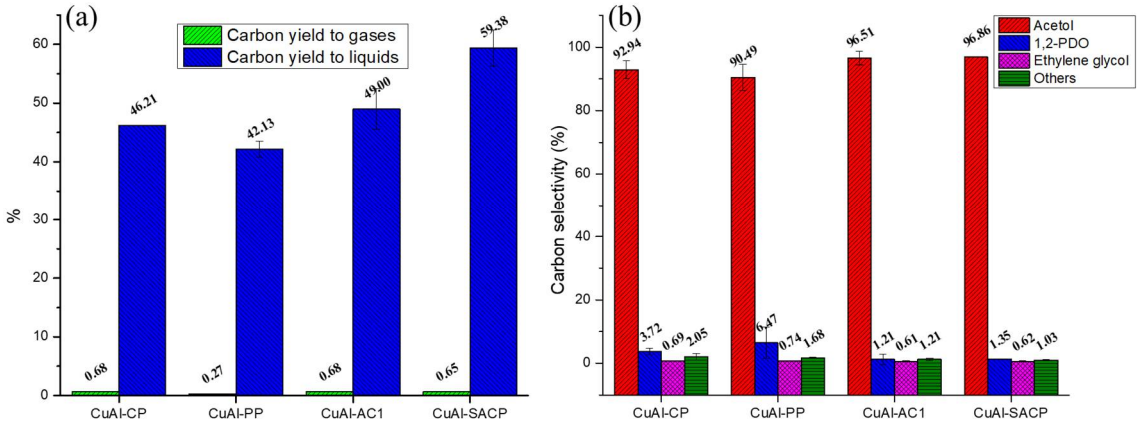

Figure 16. Catalytic performance of CuAl catalysts in the gas phase. Carbon yield to products (**a**). Carbon selectivity to liquid products (**b**). Conditions: 227 °C, 1 bar, 10 wt% glycerol, and 30 g cat min gly^{-1}.

The carbon selectivity to liquid products can be seen in Figure 16b. The main product obtained in all cases is acetol. The highest acetol selectivity is obtained from CuAl-SACP (96.86%) and CuAl-AC1 (96.51%), followed by CuAl-CP (92.94%), and CuAl-PP (90.49%). As can be seen, all catalysts are very selective to acetol. The second major product obtained is 1,2-PDO. CuAl-PP showed the highest carbon selectivity to 1,2-PDO (6.47%) followed by CuAl-CP (3.72%) > CuAl-SACP (1.35%) > CuAl-AC1 (1.21%). The carbon selectivity to ethylene glycol is also very low, with values between 0.6–0.7%. To measure the real activity of the catalysts, experiments were carried out with inert sand. The results revealed values of less than 1% of carbon yield to products. The carbon selectivity to acetol and 1,2-PDO were 22.49% and 75.43%, respectively.

The CuAl-SACP catalyst showed the highest acetol yield, with a value of 462.6 $mg_{acetol}/g_{glycerol}$, which resulted from an acceptable carbon yield to liquid and a high carbon selectivity to acetol. This result could be related to the low carbon formation (Table 2) 15.5 mg $C/g_{cat}{\cdot}g_{Reacted\ glycerol}$. The CuAl-AC1 catalyst with an acetol yield of 380.4 $mg_{acetol}/g_{glycerol}$ showed low carbon formation (15.5 mg $C/g_{cat}{\cdot}g\ g_{Reacted\ glycerol}$) and liquid product selectivity similar to that obtained with the CuAl-SACP catalyst. However, the CuAl-CP and CuAl-PP catalysts showed higher carbon formation with values of 31.8 and 27.2 mg $C/g_{cat}{\cdot}g\ g_{Reacted\ glycerol}$ and similar liquid product selectivity with lower selectivity to acetol, around 92%, and higher selectivity to 1,2-PDO, around 4%. The CuAl-PP catalyst showed the lowest acetol yield, 306.6 $mg_{acetol}/g_{glycerol}$, which is a consequence of the lower carbon yield to liquids and low carbon selectivity to acetol.

A comparison of CuAl-CP and CuAl-SACP catalysts with similar Cu content and different crystallite sizes of spent catalysts, determined by XRD (Scherrer's equation), 25.8 nm and 33.6 nm for CuAl-CP and CuAl-SACP, respectively, indicated that the larger crystallite size of the CuAl-SACP catalyst than the CuAl-CP catalyst did not adversely affect the acetol yield. Furthermore, the higher S_{BET} of the CuAl-CP catalyst than the CuAl-SACP catalyst, with values of 141 and 69 m^2/g, respectively, did not favor the acetol yield. Considering the H_2-TPR results (Figure 6), the CuAl-CP catalyst showed a higher proportion of the easily reduced CuO phase around 231 °C, while the CuAl-SACP catalyst presented a higher proportion of the reduced CuO phase at 252 °C. After activation of the catalyst with H_2, the Cu^0-Al_2O_3 assembly should be appropriate for the dehydration of glycerol to acetol in the gas phase, generating low carbon formation.

The CuAl-PP catalyst showed in the H_2-TPR analysis the greatest relative amount of reduced CuO phase at 228 °C, being the catalyst with the highest Cu crystallite size, determined by XRD, 36.2 nm, and the highest Cu content (52.2%).

The low carbon formation of CuAl-AC1 catalyst, 15.5 mg $C/g_{cat} \cdot g_{glycerol\ reacted}$ could be related to the presence of $CuAl_2O_4$ spinel phase in the calcined catalyst and, as a consequence, a relative amount of 12.1% of reduced oxidized phase at 355 °C in the H_2-TPR analysis.

Comparing these results with those obtained in the liquid phase (Figures 12 and 15), it is clear that in the gas phase the carbon selectivity to acetol is much greater than in the liquid phase. In this way, the dehydration pathway seems to be promoted instead of the sequential dehydration–hydrogenation of glycerol. This problem has been previously reported by other authors [24,27] in the liquid and gas phases. Since this phenomenon is observed in all catalysts, regardless of the preparation method, we believe that the reaction mechanism may be similar for both liquid-phase and gas-phase reactions. The differences in glycerol conversion and acetol selectivity favoring gas-phase catalysts are not primarily due to the reaction steps themselves, but rather the lower diffusivity of glycerol in the liquid phase. This reduces access to the catalyst's active sites, decreasing conversion on one hand, and on the other hand increases the contact time of adsorbed products on the catalyst surface, facilitating subsequent hydrogenation reactions of acetol and lowering its selectivity. In the gas phase, the greater diffusivity of glycerol enhances conversion to acetol, and the higher space velocity, along with shorter contact times, prevents subsequent reactions towards 1,2-PDO, thus explaining the observed increase in acetol selectivity.

However, other phenomena may also influence the catalytic results. The XRD results (Figure 4a,b) indicate that in the liquid phase, Cu^0 is oxidized, while this does not occur in the gas phase. We propose that this oxidation during the reaction facilitates electron transfer from the Cu catalyst to acetol, enhancing its hydrogenation to 1,2-PDO, as proposed by previous researchers [27].

On the other hand, textural properties also seem to influence the catalytic behavior of our catalysts. The high S_{BET} values for the catalysts after their use in the gas phase of glycerol dehydration appeared to negatively affect the performance of the catalysts. Therefore, the CuAl-CP and CuAl-PP catalysts exhibited the highest S_{BET} values but demonstrated low glycerol conversion, low acetol selectivity, and high carbon formation.

Textural properties did not appear to be significant in the dehydration of glycerol in the liquid phase. The CuAl-SACP and CuAl-PP catalysts used in the liquid phase showed the highest and lowest S_{BET} values after use, respectively, and both catalysts displayed poor catalytic performance with low glycerol conversion. In this way, diffusion problems as well as the appearance of a Cu^0/Cu^+ ratio during the reaction, influenced by the microstructure of the catalysts, seem to have a greater influence in the liquid phase.

2.4. Comparison with Other Works of Literature

Although the comparison of the performance of the catalysts shown in this work with other published works is not simple, since the operating conditions, flow rates, catalyst amounts, and other conditions are not identical from one work to another, beyond the values of conversions, selectivities, and yields, one can try to obtain an estimated reaction rate for the disappearance of glycerol by dividing the glycerol conversions of each work by the W/m ratios used and, despite all the limitations of such a simple analysis, obtain a number that allows us to compare the performance of the catalysts in a more objective way than simple conversion values. Thus, if we perform this calculation for the different published catalysts shown in Table 5 and compare them with the results of the catalysts in this work, it can be seen that while the conversion is very low in our catalysts in the liquid phase, and logically increases as the W/m increases, the kinetics of the glycerol disappearance reaction, calculated as mentioned above, is of the same order of magnitude as the catalysts in other works (from 0.169 to 0.399 g gly min^{-1} g cat^{-1}), and if what we

compare is the rate of acetol formation, this is higher for all the catalysts in this work than practically all the catalysts published in other references. The acetol rate, expressed as g glycerol reacted min^{-1} g cat^{-1}, was calculated by multiplying the glycerol rate by the acetol selectivity. The analysis of these results shows that the behavior of the catalysts in the gas phase notably improves not only the rates but also the selectivity towards the formation of acetol.

Table 5. Comparison of glycerol and acetol rates with other works in the literature.

Catalysts	Operating Conditions (T, P, $W/m_{glycerol}$)	Glycerol Conversion (%)	Acetol Yield (%)	Glycerol Rate (g gly min^{-1} g cat^{-1})	Acetol Rate (g gly min^{-1} g cat^{-1})	Ref.
20%CuNi/Al_2O_3	250 °C, 40 bar, g cat min gly^{-1}	80.0	12.0	0.262	0.039	[78]
20%Cu/Al_2O_3	"	50.0	4.5	0.164	0.015	[78]
Cu/$CuAl_2O_4$ [a]	220 °C, 20 bar, 138.9–416.7 g cat min gly^{-1}	90.0	19.8	0.216	0.048	[79]
Cu/$CuAl_2O_4$ [a]	230 °C, 20 bar, 138.9–416.7 g cat min gly^{-1}	91.0	19.1	0.218	0.046	[79]
Ni/Cu/ Al_2O_3	230 °C, 35 bar, 259.2 g cat min gly^{-1}	25.7	4.4	0.099	0.017	[80]
Ni/Cu/ Al_2O_3 [b]	"	77.9	10.7	0.301	0.041	[80]
Ni-Cu/Al_2O_3	250 °C, 40 bar, 304.9 g cat min gly^{-1}	90.0	10.0	0.295	0.033	[81]
$CuNi_{10}$/MgO-Al_2O_3	"	65.0	23.5	0.213	0.077	[81]
$CuNi_{20}$/MgO-Al_2O_3	"	60.0	23.5	0.197	0.077	[81]
$CuNi_{30}$/MgO-Al_2O_3	"	75.0	25.0	0.246	0.082	[81]
Cu:Al-1 (50:50)	220 °C, 20 bar, 170.7 g cat min gly^{-1}	91.0	47.3	0.533	0.277	[82]
CuO/Al_2O_3 [a,c]	240 °C, 1 bar, 150 g cat min gly^{-1}	78.0	35.0	0.520	0.182	[83]
Cu-Mg/Al-1 [a,c]	"	61.5	53.0	0.410	0.217	[83]
Cu-Mg/Al-2 [a,c]	"	58.0	46.5	0.387	0.180	[83]
Cu-Mg/Al-3 [a,c]	"	68.0	46.8	0.453	0.212	[83]
Cu-Mg/Al-4 [a,c]	"	68.0	55.0	0.453	0.249	[83]
Cu-Mg/Al-5 [a,c]	"	64.0	46.0	0.427	0.196	[83]
Cu-Mg/Al-6 [a,c]	"	62.5	32.0	0.417	0.133	[83]
CuAl-AC1	227 °C, 34 bar, 10 g cat min gly^{-1}	4.0	2.0	0.396	0.205	TW
CuAl-PP	"	2.2	1.4	0.220	0.138	TW
CuAl-CP	"	4.0	2.0	0.399	0.199	TW
CuAl-SACP	"	2.5	1.3	0.247	0.128	TW
CuAl-PP	227 °C, 34 bar, 30 g cat min gly^{-1}	5.1	2.8	0.169	0.095	TW
CuAl-CP	"	7.9	2.9	0.262	0.096	TW
CuAl-AC1 [a]	227 °C, 1 bar, 30 g cat min gly^{-1}	49.7	47.9	1.656	1.598	TW
CuAl-PP [a]	"	42.4	38.4	1.413	1.279	TW
CuAl-CP [a]	"	46.9	43.6	1.563	1.453	TW
CuAl-SACP [a]	"	60.0	58.1	2.001	1.938	TW

TW: this work [a] Gas phase, [b] 2-propanol as feed solvent, [c] Methanol as feed solvent. " same value as the previous one.

3. Materials and Methods

3.1. Materials

The materials employed were $Cu(NO_3)_2 \cdot 3H_2O$ (Sigma-Aldrich, St. Louis, MO, USA, purity: 99.99%), $Al(NO_3)_3 \cdot 9H_2O$ (Thermo Scientific, Waltham, MA, USA, purity: >98%), citric acid (Labkem, Dublin, Ireland, purity: 99.7–100.3%), ethylene glycol (Labkem, purity: >99%), ethanol (Panreac AppliChem, Darmstadt, Germany, purity: 96%), milliQ water, NH_4OH (Carlo Erba, Cornaredo, Italy, purity: 30%), CTAB (Sigma Aldrich, purity: ≥98%), and citric acid (Labkem, purity: 99.7–100.3%).

3.2. Catalysts Preparation

The CuAl catalysts with a Cu:Al molar ratio of 1:1 were prepared following four different methods: CP, SACP, AC, and PP.

CuAl-AC1 was prepared by AC according to previous reports [47–50], using citric acid as a combustion agent. This preparation method consists of preparing an aqueous solution containing metallic nitrates ($Cu(NO_3)_2 \cdot 3H_2O$ and $Al(NO_3)_3 \cdot 9H_2O$) and citric acid. The amount of citric acid used was previously determined from the work of Jain et al. [84] using a value of the parameter φ equal to 1. Then, a proportion of 0.24 mol of $Cu(NO_3)_2 \cdot 3H_2O$, 0.24 mol $Al(NO_3)_3 \cdot 9H_2O$, and 0.33 mol of citric acid in 200 mL of mili-Q water was employed. The solution was heated up to 150 °C until it became a viscous gel. At this point, the gel was heated up to 300 °C until the ignition point was reached. After the ignition point, a solid material was generated.

The CuAl-CP catalyst was prepared via a coprecipitation method employing an NH_4OH aqueous solution as a precipitant agent, as described in previous reports [13]. During this preparation 0.5 mol of $Cu(NO_3)_2 \cdot 3H_2O$ and 0.5 mol $Al(NO_3)_3 \cdot 9H_2O$ were dissolved in mili-Q water, heated up to 40 °C, and maintained under stirring at this temperature. The precipitant agent was added dropwise until a pH of 6.2 was reached. This pH value was selected to achieve the total incorporation of Cu, as had been studied in previous works [85]. Finally, the precipitate was filtered.

The procedure followed for the synthesis of CuAl-SACP catalyst was similar to that described in CuAl-CP. Previous to the addition of the precipitant, a desired amount of CTAB was added to the mixture. The molar CTAB/metal ratio, 1:4, was selected from the work of Hu et al. [86].

The CuAl-PP catalyst was prepared following the procedure described in several previous works, such as [44,45]. This synthesis started from two different solutions: one was an aqueous solution containing 0.5 mol of $Cu(NO_3)_2 \cdot 3H_2O$ and 0.5 mol of $Al(NO_3)_3 \cdot 9H_2O$, while the other solution was composed of ethanol and a desired amount of citric acid (CA), maintaining a 2:1 CA/metal molar ratio. In a second step, both solutions were mixed and maintained at 60 °C under vigorous stirring for 60 min. After this time under stirring, a desired amount of ethylene glycol (EG) was added to the mixture, setting a 2:3 CA/EG mass ratio, and the mixture was heated up to 100 °C for 12 h until it became a viscous resin.

All prepared materials were dried overnight at 105 °C (except CuAl-AC1, which does not need a drying step), calcined at 650 °C for 3 h, and sieved to a particle size of 160–315 μm.

A descriptive scheme with the key points of each preparation method can be seen in Figure 17.

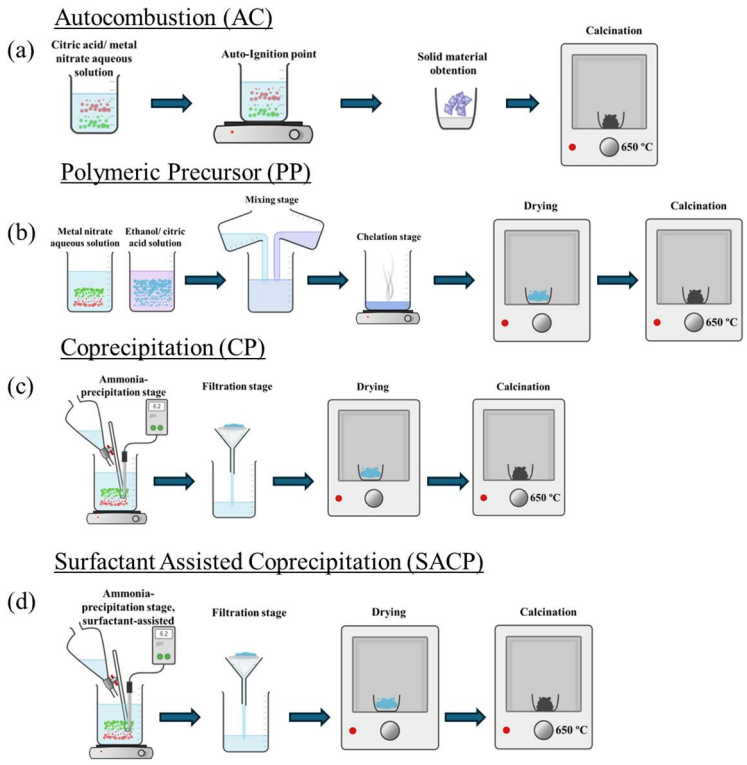

Figure 17. Scheme of the different preparation methods: auto-combustion (**a**), polymeric precursor (**b**), coprecipitation (**c**), and surfactant-assisted coprecipitation (**d**).

3.3. Catalysts Characterization

The calcined, reduced, and used catalysts were analyzed by X-ray diffraction (XRD) in a RIGAKU D/max 2500 diffractometer (Tokyo, Japan) which was equipped with a Cu Kα radiation (λ = 0.15418 nm) and a graphite monochromator operated at atmospheric temperature, 40 kV, and 80 mA. Samples were scanned from 5° to 90° (2θ) at a rate of 0.03°/s. Phase identification was conducted employing JCPDS cards.

N_2 adsorption–desorption isotherms analyses were conducted in order to study the textural properties of the prepared materials. Analyses were carried out employing a Quantachrome Autosorb iQ3 TPX instrument (Boothwyn, PA, USA). Previous to the analyses, samples were outgassed at 350 °C and 10^{-3} mmHg for 15 h in order to remove physically adsorbed impurities. The specific surface area (S_{BET}) was determined by the BET method, while the pore size distribution was calculated using the BJH method at the adsorption branch.

H_2-TPR profiles were obtained on a Micromeritic Autochem II 2920 instrument (Norcross, GA, USA) equipped with a thermal conductivity detector (TCD). Around 150 mg of each sample was firstly pretreated in an Ar stream at 150 °C for 30 min (heating rate 10 °C/min, total flow 50 mL/min) with the aim of completely eliminating moisture. Then, the catalyst was reduced by passing a 10%H_2-Ar 50 mL/min total flow while the temperature was increased up to 950 °C with a heating rate of 10 °C/min.

The metal loadings in each catalyst were determined by inductively coupled plasma optical emission spectrometry (ICP-OES). Previous to the analysis, calcined samples were subjected to microwave digestion employing a mixture of HNO_3 and HCl. ICP-OES was also employed to study the metal leaching during the reaction. For this analysis, a representative sample of the product aqueous solution from each experiment was used. With the aim of determining the carbon deposition on the catalysts, the elemental analysis with a LECO CHN 628 instrument (St. Joseph, MI, USA) of the used catalysts was carried out. Samples of around 30 mg were employed in each assessment.

The surface morphology of the catalysts was studied by field emission scanning electron microscopy (FESEM). These measurements were carried out using a Carl Zeiss MERLIN^{TM} (Oberkochen, Germany) equipped with secondary and backscattered electron detectors in the chamber and column (in-lens). In addition, it was equipped with an EDS detector (INCA 350 from Oxford Instruments (Bucks, UK) with an energy resolution of 127 eV at 5.9 keV) for qualitative chemical analysis.

In order to study and quantify the transformation of Al_2O_3 (or non-stoichiometric alumina $Al_{2.667}O_4$) into boehmite, TGA analyses were performed. Weight loss is directly related to boehmite formation [87]. These analyses were carried out using a heating ramp of 5 °C/min under a N_2 atmosphere.

X-ray photoelectron spectroscopy (XPS) and X-ray excited Auger electron spectroscopy (XAES) were conducted with the aim of studying the Cu/Al surface ratio, as well as the chemical states of the Cu and Al, respectively. The measurements were done using an ESCAPlus Omicron (Taunusstein, Germany) with a monochromatic Al Kα (1486.7 eV) radiation source. The obtained signals were deconvoluted after Tougaard background subtraction, employing a mixed Gaussian–Lorentzian function. The binding energies (BEs) were calibrated setting C 1s of adventitious carbon as a reference at 284.8 eV. The concentration of the surface elements was determined by adjusting the values with relative atomic sensitivity factors of previous studies [88].

3.4. Catalyst Tests

The selective dehydration of glycerol in the liquid phase was evaluated using a laboratory-scale continuous feeding unit designed and developed by PID (Process Integral Development Eng & Tech, Alcobendas, Spain). The schematic diagram of the pressurized experimental system is shown in Figure 18a. This experimental system has a stainless steel tubular reactor (Autoclave Engineers, Erie, PA, USA) with an inner diameter of 9 mm. The bed, inside the reactor, is placed between quartz wool supports and consists of a mixture of inert sand (with a particle size higher than 315 μm) and catalyst (with a particle size between 315–160 μm). An up-flow liquid feed, consisting of a 10%wt glycerol mixture with deionized water, is fed by means of a high-performance liquid chromatography (HPLC) pump. In order to pressurize the system and control the system's pressure, an Equilibar LF Series Precision Back Pressure Regulator (Fletcher, NC, USA) was employed.

The outlet stream from the top of the reactor, consisting of a mixture of gas and liquid products, was depressurized by the backpressure regulator and passed to the condensation system, which consisted of a set of four condensers placed in an ice bath. The first one was used to collect the water during the stabilization of the reaction conditions. The next two condensers were used to collect the liquid products obtained during the first and second hour of the experiment (each experiment had a length of two hours). The fourth condenser was used to collect the remaining products.

The gas flow exiting from the condensation system was analyzed with an Agilent 490 Micro GC (Santa Clara, CA, USA) equipped with a molecular sieve column, a Plot U, and Thermal Conductivity Detectors (TCDs), where N_2, H_2, CH_4, CO_2, CO, C_2H_6, and C_3H_8 were quantified. A N_2 gas flow of 75 cm^3 (STP)/min was fed by means of a mass flow controller (Hi-Tec Bronkhorst, Ruurlo, The Netherlands) during the reaction after the backpressure regulator, and this was used as an internal standard.

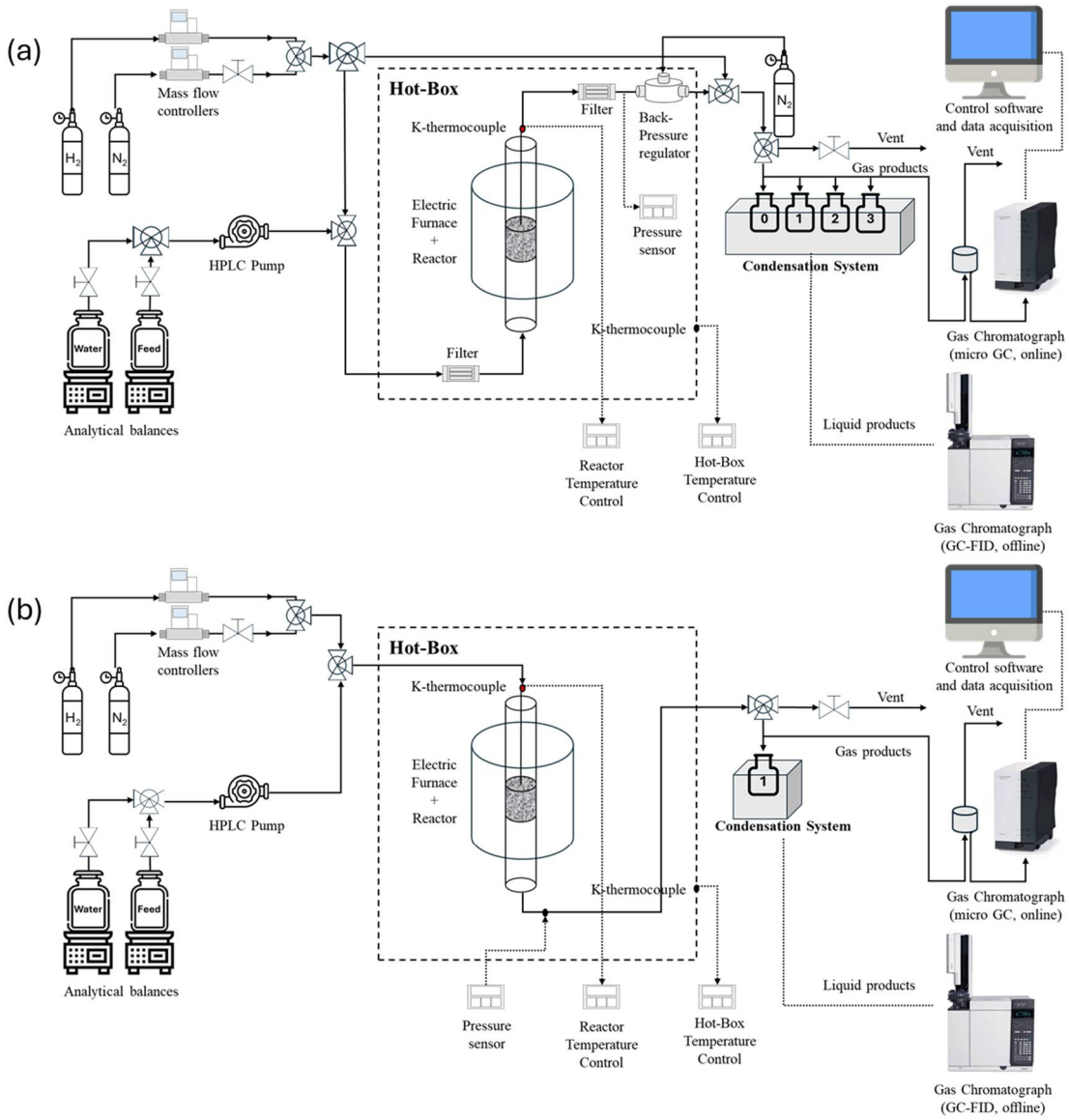

Figure 18. Schematic diagram of the pressurized (liquid phase) experimental system (**a**) and the atmospheric (gas phase) experimental system (**b**).

The liquid products collected in the condensation system were analyzed off-line with an Agilent 7820A GC, equipped with a Flame Ionization Detector (FID) and a HP-FFAP Agilent 19091F-105 capillary column, where acetaldehyde, acetone, acrolein, methanol (MeOH), isopropanol, ethanol (EtOH), acetol, acetic acid (AA), 1,2-propanediol (1,2-PDO), ethylene glycol (EG), and unreacted glycerol were quantified. Additionally, 1-butanol was used as internal standard with the aim of reducing the error derived from sample injection variations. The injector and detector temperatures were 275 °C and 300 °C, respectively.

The selective dehydration of glycerol in the gas phase was studied using another laboratory-scale continuous feeding unit designed and developed by PID (Process Integral Development Eng & Tech, Spain). The schematic diagram of the atmospheric experimental system is shown in Figure 18b. This experimental system has a quartz tubular reactor with an inner diameter of 10.0 mm. The reaction bed is placed at a height of 150 mm in the center of the reactor. This bed is composed of 0.6 g of catalysts supported on quartz wool. A 10%wt glycerol aqueous solution was continuously pumped into the reactor with a HPLC pump. Before entering the reactor, the liquid stream was mixed with a gas flow of 40 mL/min of N_2, with the aim of using it as an internal standard for the gaseous

products and as carrier gas for the liquid mixture. The stream from the lower part of the reactor, composed of a mixture of gas and liquid products, passed through a condensation system where liquid products were collected. This condensation system consisted of a condenser immersed in an ice bath. The outlet gas flow was analyzed on-line employing the same system as described above. The collected liquid products from the two hours experiment were collected in one condenser and analyzed following the same procedure described above.

Catalytic tests in the pressurized system were performed using the same operating conditions, 227 °C and 34 absolute bar, in order to study the effect of the catalyst preparation method. The amounts of catalyst used were 1 and 3 g, which correspond to the catalyst/glycerol mass flow rate (W/m) ratios of 10 and 30 $g_{catalyst}{\cdot}min{\cdot}g_{glycerol}{}^{-1}$, respectively. The reaction bed, comprised of catalyst mixed with sand, maintained a constant bed volume of 5.5 cm^3. A solution of 10%wt glycerol in mili-Q water with a liquid flow rate of 1 mL/min was used as liquid feed.

Catalytic tests in the atmospheric system were also conducted at 227 °C. These experiments were performed using 0.6 g of catalyst and a liquid flow rate of 0.2 mL/min of a solution of 10wt% glycerol in mili-Q water, which corresponds to a W/m ratio of 30 $g_{catalyst}{\cdot}min{\cdot}g_{glycerol}{}^{-1}$. In both systems, each catalyst was tested three times in order to check their repeatability.

Prior to the reaction, each catalyst was reduced. The activation was carried out in situ, using a H_2 stream of 100 cm^3 (STP)/min during 1 h at temperatures of 300 °C for the CuAl-CP, CuAl-SACP, and CuAl-PP catalysts and 350 °C for the CuAl-AC1 catalyst. The reduction temperatures were selected according to the H_2-TPR results. The catalysts were reduced to obtain the active phase, which increases significantly the conversion of glycerol [15].

The catalytic performance was evaluated using the parameters calculated according to Equations (1)–(4).

The carbon yield to gases and carbon yield to liquids were calculated following Equations (1) and (2), respectively:

$$Carbon\ yield\ to\ gas(\%) = \frac{n(CO2) + n(CO) + n(CH4) + 2{\cdot}n(C2H6) + 3{\cdot}n(C3H8)}{3{\cdot}n(gly)in} \times 100; \quad (1)$$

$$Carbon\ yield\ to\ liquid(\%) = \frac{\begin{array}{l}2{\cdot}n(Acetaldehyde) + 3{\cdot}n(Acetone) + 3{\cdot}n(Acrolein) + n(MeOH) + 3{\cdot}n(Isopropanol) + \\ 2{\cdot}n(EtOH) + 3{\cdot}n(Acetol) + 2{\cdot}n(AA) + 3{\cdot}n(1,2-PDO) + 2{\cdot}n(EG)\end{array}}{3{\cdot}n(gly)in} \times 100; \quad (2)$$

where n_i refers to the mol of every gaseous or liquid obtained product and n(gly)in refers to the mol of glycerol fed into the reactor.

In this work, we assume that the glycerol conversion, named effective activity (Equation (3)), is the addition of the carbon yield to gas and carbon yield to liquid. We use "effective activity" due to some difficulties during glycerol analysis. These difficulties originated from glycerol polymerization, obstruction, or retention over catalysts' surfaces, as were also observed in other studies [83].

$$Effective\ activity\ (\%) = Carbon\ yield\ to\ gas + Carbon\ yield\ to\ liquid; \quad (3)$$

Selectivity to each liquid product is determined by Equation (4):

$$Selectivity(\%) = \frac{nf(i)}{nf(total\ products)} \times 100 \quad (4)$$

where n(f)i is the total molar amount of carbon detected from a product i, while nf(total products) refers to the total amount of carbon calculated from all the quantified products, both determined by GC-FID.

The carbon recovery in each experiment was calculated as the addition of carbon present in the gas and in liquid products together with the carbon retained in the used catalysts, related to the carbon fed in the glycerol. The carbon in liquid products was determined by a Total Organic Carbon Analyzer (TOC-L, Shimadzu Instrument, Kyoto, Japan), while the retained carbon of the used catalysts was obtained by elemental analysis.

4. Conclusions

CuAl catalysts were prepared by four methods, CP, PP, AC1, and SACP, and tested in the catalytic dehydration of glycerol to acetol. The catalyst preparation method influenced the textural properties, crystalline phases, and reducibility. The catalysts with a combustion stage in the preparation method, the CuAl-AC1 and CuAl-PP catalysts, presented a $CuAl_2O_4$ spinel phase in the calcined catalyst and a higher reduction temperature.

The catalytic conversion of glycerol showed higher yields to products and higher selectivity to acetol in the gas phase than in the liquid phase. In the liquid phase with a W/m ratio of 10 g cat min gly^{-1}, the carbon yield to products was less than 5% for all prepared CuAl catalysts. All catalysts used in the liquid phase showed boehmite and Cu_2O phases. The catalytic activity could be related to the size of the Cu crystallites and a Cu^0/Cu^+ ratio on the catalyst surface of around 0.6. The highest carbon selectivity to acetol in the liquid phase was obtained with the CuAl-PP catalyst. Increasing the W/m ratio to 30 g catalyst min g $glycerol^{-1}$ slightly increased the total yield to products, while the carbon selectivity to acetol decreased.

In the gas phase, the total carbon yield was greater than 40% and the carbon selectivity to acetol was greater than 90%. The catalyst with the best performance in the gas phase was CuAl-SACP, 462.6 $mg_{acetol}/g_{glycerol}$, which could be due to the low carbon formation and its reducible properties.

As our results indicate, acetol production appears to be more favorable in the gas phase. This suggests that a gas-phase system may be more suitable for the catalytic dehydration of glycerol. However, it is important to consider the significant energy costs associated with water vaporization in this process, which could substantially increase overall production costs. Furthermore, the formation of carbon deposits must be taken into account, as they can deactivate the catalyst and negatively affect the efficiency of the process.

On the other hand, the liquid-phase process offers energy savings by eliminating water vaporization. Nevertheless, it results in lower yields of liquid products and reduced selectivity toward acetol, which may lead to additional costs due to the need for subsequent separation steps.

Therefore, further research is necessary to determine which process configuration (gas or liquid phase) offers the best balance between yield, selectivity, and economic viability for the selective dehydration of glycerol to acetol.

Author Contributions: Conceptualization, F.M.-M. and L.G.; methodology, L.G. and J.R.; validation, F.M.-M.; formal analysis, F.M.-M. and J.R.; investigation, F.M.-M.; writing—original draft preparation, F.M.-M.; writing—review and editing, L.G., J.R., M.O. and J.A.; visualization, F.M.-M.; supervision, L.G., J.R. and J.A.; project administration, L.G.; funding acquisition, L.G., J.R., M.O. and J.A. All authors have read and agreed to the published version of the manuscript.

Funding: Grant PID2020-114985RBI00 funded by MICIU/AEI/10.13039/501100011033. The predoctoral aid granted to Francisco Maldonado Martín PRE2021-100578 funded by MICIU/AEI/10.13039/501100011033 and by ESF+. Funding from the Government of Aragón (Research Group Ref. T22_23R) is also appreciated.

Data Availability Statement: The original contributions presented in this study are included in the article. Further inquiries can be directed to the corresponding author.

Acknowledgments: The authors would like to acknowledge the use of the Servicio General de Apoyo a la Investigación-SAI of the Universidad de Zaragoza.

Conflicts of Interest: The authors declare no conflicts of interest.

References

1. When Will Fossil Fuels Run out? Available online: https://group.met.com/en/mind-the-fyouture/mindthefyouture/when-will-fossil-fuels-run-out (accessed on 14 December 2023).
2. Gebremariam, S.; Marchetti, J. Economics of Biodiesel Production: Review. *Energy Convers. Manag.* **2018**, *168*, 74–84. [CrossRef]
3. Climent, M.J.; Corma, A.; Iborra, S. Conversion of Biomass Platform Molecules into Fuel Additives and Liquid Hydrocarbon Fuels. *Green Chem.* **2014**, *16*, 516–547. [CrossRef]
4. Raso, R.; Abad, E.; García, L.; Ruiz, J.; Oliva, M.; Arauzo, J. Renewable Hydrogen Production by Aqueous Phase Reforming of Pure/Refined Crude Glycerol over Ni/Al-Ca Catalysts. *Molecules* **2023**, *28*, 6695. [CrossRef] [PubMed]
5. Faba, L.; Díaz, E.; Ordóñez, S. Aqueous-Phase Furfural-Acetone Aldol Condensation over Basic Mixed Oxides. *Appl. Catal. B* **2012**, *113–114*, 201–211. [CrossRef]
6. Hoekman, S.K.; Robbins, C. Review of the Effects of Biodiesel on NOx Emissions. *Fuel Process. Technol.* **2012**, *96*, 237–249. [CrossRef]
7. Apostolakou, A.A.; Kookos, I.K.; Marazioti, C.; Angelopoulos, K.C. Techno-Economic Analysis of a Biodiesel Production Process from Vegetable Oils. *Fuel Process. Technol.* **2009**, *90*, 1023–1031. [CrossRef]
8. Mulugetta, Y. Evaluating the Economics of Biodiesel in Africa. *Renew. Sustain. Energy Rev.* **2009**, *13*, 1592–1598. [CrossRef]
9. Pagliaro, M.; Ciriminna, R.; Kimura, H.; Rossi, M.; Della Pina, C. From Glycerol to Value-Added Products. *Angew. Chem.Int. Ed.* **2007**, *46*, 4434–4440. [CrossRef]
10. OECD-FAO. *Food and Agriculture Organization of the United Nations*; OECD Publication: Paris, France, 2011. [CrossRef]
11. Sabokmalek, S.; Alavi, S.M.; Rezaei, M.; Akbari, E. Fabrication and Catalytic Evaluation of Ni/CaO–Al_2O_3 in Glycerol Steam Reforming: Effect of Ni Loading. *J. Energy Inst.* **2023**, *109*, 101270. [CrossRef]
12. Yuan, Z.; Wang, L.; Wang, J.; Xia, S.; Chen, P.; Hou, Z.; Zheng, X. Hydrogenolysis of Glycerol over Homogenously Dispersed Copper on Solid Base Catalysts. *Appl. Catal. B* **2011**, *101*, 431–440. [CrossRef]
13. Raso, R.; García, L.; Ruiz, J.; Oliva, M.; Arauzo, J. Aqueous Phase Hydrogenolysis of Glycerol over Ni/Al-Fe Catalysts Without External Hydrogen Addition. *Appl. Catal. B* **2021**, *283*, 119598. [CrossRef]
14. Prather, M.; SSausen, R.; Houghton, J.; Penner, J.; Isaksen, I.; Wang, W.; Dorland, R. *Potential Climate Change from Aviation 6*; Cambridge University Press: Cambridge, UK, 1999; Volume 1, pp. 231–266.
15. Mane, R.B.; Yamaguchi, A.; Malawadkar, A.; Shirai, M.; Rode, C.V. Active Sites in Modified Copper Catalysts for Selective Liquid Phase Dehydration of Aqueous Glycerol to Acetol. *RSC Adv.* **2013**, *3*, 16499–16508. [CrossRef]
16. Corma, A.; Huber, G.W.; Sauvanaud, L.; O'Connor, P. Biomass to Chemicals: Catalytic Conversion of Glycerol/Water Mixtures into Acrolein, Reaction Network. *J. Catal.* **2008**, *257*, 163–171. [CrossRef]
17. Sato, S.; Akiyama, M.; Takahashi, R.; Hara, T.; Inui, K.; Yokota, M. Vapor-Phase Reaction of Polyols over Copper Catalysts. *Appl. Catal. A Gen.* **2008**, *347*, 186–191. [CrossRef]
18. Sato, S.; Sakai, D.; Sato, F.; Yamada, Y. Vapor-Phase Dehydration of Glycerol into Hydroxyacetone over Silver Catalyst. *Chem. Lett.* **2012**, *41*, 965–966. [CrossRef]
19. Dieuzeide, M.L.; Jobbagy, M.; Amadeo, N. Vapor-Phase Hydrogenolysis of Glycerol to 1,2-Propanediol over Cu/Al_2O_3 Catalyst at Ambient Hydrogen Pressure. *Ind. Eng. Chem. Res.* **2016**, *55*, 2527–2533. [CrossRef]
20. Pandhare, N.N.; Pudi, S.M.; Biswas, P.; Sinha, S. Selective Hydrogenolysis of Glycerol to 1,2-Propanediol over Highly Active and Stable Cu/MgO Catalyst in the Vapor Phase. *Org. Process. Res. Dev.* **2016**, *20*, 1059–1067. [CrossRef]
21. Pandhare, N.N.; Pudi, S.M.; Biswas, P.; Sinha, S. Vapor Phase Hydrogenolysis of Glycerol to 1,2-Propanediol over γ-Al_2O_3 Supported Copper or Nickel Monometallic and Copper-Nickel Bimetallic Catalysts. *J. Taiwan Inst. Chem. Eng.* **2016**, *61*, 90–96. [CrossRef]
22. Yin, A.Y.; Guo, X.Y.; Dai, W.L.; Fan, K.N. The Synthesis of Propylene Glycol and Ethylene Glycol from Glycerol Using Raney Ni as a Versatile Catalyst. *Green Chem.* **2009**, *11*, 1514–1516. [CrossRef]
23. Nakagawa, Y.; Tomishige, K. Heterogeneous Catalysis of the Glycerol Hydrogenolysis. *Catal. Sci. Technol.* **2011**, *1*, 179–190. [CrossRef]
24. Lete, A.; Raso, R.; García, L.; Ruiz, J.; Arauzo, J. Synthesis of Ketones from Glycerol and 1,2-Propanediol Using Copper and Nickel Catalysts: Unraveling the Impact of Reaction Phase and Active Metal. *Fuel* **2024**, *371*, 132001. [CrossRef]

25. Farias, M.F.; Domingos, Y.S.; Turolla Fernandes, G.J.; Castro, F.L.; Fernandes, V.J.; Fonseca Costa, M.J.; Araujo, A.S. Effect of Acidity in the Removal-Degradation of Benzene in Water Catalyzed by Co-MCM-41 in Medium Containing Hydrogen Peroxide. *Microporous Mesoporous Mater.* **2018**, *258*, 33–40. [CrossRef]
26. Wen, G.; Xu, Y.; Ma, H.; Xu, Z.; Tian, Z. Production of Hydrogen by Aqueous-Phase Reforming of Glycerol. *Int. J. Hydrogen Energy* **2008**, *33*, 6657–6666. [CrossRef]
27. Xiao, Z.; Wang, X.; Xiu, J.; Wang, Y.; Williams, C.T.; Liang, C. Synergetic Effect between Cu 0 and Cu + in the Cu-Cr Catalysts for Hydrogenolysis of Glycerol. *Catal. Today* **2014**, *234*, 200–207. [CrossRef]
28. Lopez-Pedrajas, S.; Estevez, R.; Blanco-Bonilla, F.; Luna, D.; Bautista, F.M. Insight into the Gas-Phase Glycerol Dehydration on Transition Metal Modified Aluminium Phosphates and Zeolites. *J. Chem. Technol. Biotechnol.* **2017**, *92*, 2661–2672. [CrossRef]
29. Gharibi Kharaji, A.; Beheshti, M.; Repke, J.U.; Tangestani-nejad, S.; Görke, O.; Godini, H.R. Using Response Surface Method to Analyze the Effect of Hydrothermal Post-Treatment on the Performance of Extrudates HZSM-5 Catalyst in the Methanol to Propylene Reaction. *React. Kinet. Mech. Catal.* **2019**, *127*, 375–390. [CrossRef]
30. Zhou, M.; Zhang, L.; Lu, H.; Shao, L.; Chen, M. Reaction of Silicon Dioxide with Water: A Matrix Isolation Infrared and Density Functional Theoretical Study. *J. Mol. Struct.* **2002**, *605*, 249–254. [CrossRef]
31. Wolosiak-Hnat, A.; Milchert, E.; Grzmil, B. Influence of Parameters on Glycerol Hydrogenolysis over a Cu/Al_2O_3 Catalyst. *Chem. Eng. Technol.* **2013**, *36*, 411–418. [CrossRef]
32. Zhou, J.; Guo, L.; Guo, X.; Mao, J.; Zhang, S. Selective Hydrogenolysis of Glycerol to Propanediols on Supported Cu-Containing Bimetallic Catalysts. *Green Chem.* **2010**, *12*, 1835–1843. [CrossRef]
33. Suprun, W.; Lutecki, M.; Haber, T.; Papp, H. Acidic Catalysts for the Dehydration of Glycerol: Activity and Deactivation. *J. Mol. Catal. A Chem.* **2009**, *309*, 71–78. [CrossRef]
34. Kang, S.H.; Bae, J.W.; Sai Prasad, P.S.; Park, S.J.; Woo, K.J.; Jun, K.W. Effect of Preparation Method of Fe-Based Fischer-Tropsch Catalyst on Their Light Olefin Production. *Catal. Lett.* **2009**, *130*, 630–636. [CrossRef]
35. Santos, R.C.R.d.; da Silva Júnior, M.J.; Nunes, G.L.; Valentini, A. Effect of Cu and Sb Active Sites on the Acid-Base Properties and Reactivity of Hydrated Alumina for Glycerol Conversion by Dehydrogenation and Dehydration Reactions. *Catal. Sci. Technol.* **2023**, *13*, 4223–4245. [CrossRef]
36. Liu, Y.; Guo, X.; Rempel, G.L.; Ng, F.T.T. The Promoting Effect of Ni on Glycerol Hydrogenolysis to 1,2-Propanediol with in Situ Hydrogen from Methanol Steam Reforming Using a $Cu/Zno/Al_2O_3$ Catalyst. *Catalysts* **2019**, *9*, 412. [CrossRef]
37. Basag, S.; Piwowarska, Z.; Kowalczyk, A.; Węgrzyn, A.; Baran, R.; Gil, B.; Michalik, M.; Chmielarz, L. Cu-Mg-Al Hydrotalcite-like Materials as Precursors of Effective Catalysts for Selective Oxidation of Ammonia to Dinitrogen—The Influence of Mg/Al Ratio and Calcination Temperature. *Appl. Clay Sci.* **2016**, *129*, 122–130. [CrossRef]
38. Chiu, C.W.; Dasari, M.A.; Suppes, G.J.; Sutterlin, W.R. Dehydration of Glycerol to Acetol via Catalytic Reactive Distillation. *AIChE J.* **2006**, *52*, 3543–3548. [CrossRef]
39. Chu, Z.; Chen, H.; Yu, Y.; Wang, Q.; Fang, D. Surfactant-Assisted Preparation of $Cu/ZnO/Al_2O_3$ Catalyst for Methanol Synthesis from Syngas. *J. Mol. Catal. A Chem.* **2013**, *366*, 48–53. [CrossRef]
40. Alvar, E.N.; Rezaei, M.; Alvar, H.N. Synthesis of Mesoporous Nanocrystalline $MgAl_2O_4$ Spinel via Surfactant Assisted Precipitation Route. *Powder Technol.* **2010**, *198*, 275–278. [CrossRef]
41. Das, D.; Llorca, J.; Dominguez, M.; Colussi, S.; Trovarelli, A.; Gayen, A. Methanol Steam Reforming Behavior of Copper Impregnated over CeO_2–ZrO_2 Derived from a Surfactant Assisted Coprecipitation Route. *Int. J. Hydrogen Energy* **2015**, *40*, 10463–10479. [CrossRef]
42. Kang, H.T.; Zhang, C.Y.; Lv, K.; Yuan, S.L. Surfactant-Assisted Synthesis and Catalytic Activity for SOx Abatement of High-Surface-Area CuMgAlCe Mixed Oxides. *Ceram. Int.* **2014**, *40*, 5357–5363. [CrossRef]
43. Charisiou, N.D.; Italiano, C.; Pino, L.; Sebastian, V.; Vita, A.; Goula, M.A. Hydrogen Production via Steam Reforming of Glycerol over Rh/γ-Al_2O_3 Catalysts Modified with CeO_2, MgO or La_2O_3. *Renew. Energy* **2020**, *162*, 908–925. [CrossRef]
44. Braga, T.P.; Essayem, N.; Valentini, A. Correlation Between the Basicity of Cu–MxOy–Al_2O_3 (M = Ba, Mg, K or La) Oxide and the Catalytic Performance in the Glycerol Conversion from Adsorption Microcalorimetry Characterization. *J. Therm. Anal. Calorim.* **2017**, *129*, 65–74. [CrossRef]
45. Dang, H.T.; Le, T.K. Precursor Chain Length Dependence of Polymeric Precursor Method for the Preparation of Magnetic Fenton-like $CuFe_2O_4$-Based Catalysts. *J. Solgel. Sci. Technol.* **2016**, *80*, 160–167. [CrossRef]
46. Braga, T.P.; Essayem, N.; Prakash, S.; Valentini, A. Gas-Phase Conversion of Glycerol to Acetol: Influence of Support Acidity on the Catalytic Stability and Copper Surface Properties on the Activity. *J. Braz. Chem. Soc.* **2016**, *27*, 2361–2371. [CrossRef]
47. Qi, X.; Zhou, J.; Yue, Z.; Gui, Z.; Li, L. Auto-Combustion Synthesis of Nanocrystalline $LaFeO_3$. *Mater. Chem. Phys.* **2002**, *78*, 25–29.
48. Kumar, M.; Srikanth, S.; Ravikumar, B.; Lex, T.; Das, S. Synthesis of Pure and Sr-Doped $LaGaO_3$, $LaFeO_3$ and $LaCoO_3$ and Sr,Mg-Doped $LaGaO_3$ for ITSOFC Application Using Different Wet Chemical Routes. *Mater. Chem. Phys.* **2009**, *113*, 803–815. [CrossRef]

49. Kondakindi, R.R.; Karan, K.; Peppley, B.A. A Simple and Efficient Preparation of $LaFeO_3$ Nanopowders by Glycine-Nitrate Process: Effect of Glycine Concentration. *Ceram. Int.* **2012**, *38*, 449–456. [CrossRef]
50. Velasquez, M.; Santamaria, A.; Batiot-Dupeyrat, C. Selective Conversion of Glycerol to Hydroxyacetone in Gas Phase over La_2CuO_4 Catalyst. *Appl. Catal. B* **2014**, *160*, 606–613. [CrossRef]
51. Beck, M.T.; Nagypál, I. Chemistry of Complex Equilibria. *Ellis Horwood Ser. Inorg. Chem.* **1990**, *95*, 647–648.
52. Diachenko, O.; Kováč, J.; Dobrozhan, O.; Novák, P.; Kováč, J.; Skriniarova, J.; Opanasyuk, A. Structural and Optical Properties of Cuo Thin Films Synthesized Using Spray Pyrolysis Method. *Coatings* **2021**, *11*, 1392. [CrossRef]
53. Rajesh Ch, L.; Rao, N.M. A Solid-State Reaction Based Study, Synthesis and Characterization for $CuAl_2O_4$ Nanocrystalline Powder. *Optik* **2023**, *294*, 171472. [CrossRef]
54. Solache-Carranco, H.; Juárez-Díaz, G.; Martínez-Juárez, J.; Peña-Sierra, R. Estudio de La Cristalización de Cu_2O y Su Caracterización Por Difracción de Rayos X, Espectroscópica Raman y Fotoluminiscencia. *Rev. Mex. Física* **2009**, *55*, 393–398.
55. Jiménez, J.A.; Padilla, I.; Lõpez-Delgado, A.; Fillali, L.; Lõpez-Andrés, S. Characterization of the Aluminas Formed during the Thermal Decomposition of Boehmite by the Rietveld Refinement Method. *Int. J. Appl. Ceram. Technol.* **2015**, *12*, E178–E186. [CrossRef]
56. Mane, R.B.; Kondawar, S.E.; Niphadkar, P.S.; Joshi, P.N.; Patil, K.R.; Rode, C. V Effect of Preparation Parameters of Cu Catalysts on Their Physico-Chemical Properties and Activities for Glycerol Hydrogenolysis. *Catal. Today* **2012**, *198*, 321–329. [CrossRef]
57. Vasiliadou, E.S.; Lemonidou, A.A. Investigating the Performance and Deactivation Behaviour of Silica-Supported Copper Catalysts in Glycerol Hydrogenolysis. *Appl. Catal. A Gen.* **2011**, *396*, 177–185. [CrossRef]
58. Rao, R.; Dandekar, A.; Baker, R.T.K.; Vannice, M.A. Properties of Copper Chromite Catalysts in Hydrogenation Reactions. *J. Catal.* **1997**, *171*, 406–419. [CrossRef]
59. Khasin, A.A.; Yur'Eva, T.M.; Plyasova, L.M.; Kustova, G.N.; Jobic, H.; Ivanov, A.; Chesalov, Y.A.; Zaikovskii, V.I.; Khasin, A.V.; Davydova, L.P.; et al. Mechanistic Features of Reduction of Copper Chromite and State of Absorbed Hydrogen in the Structure of Reduced Copper Chromite. *Russ. J. Gen. Chem.* **2008**, *78*, 2203–2213. [CrossRef]
60. El Doukkali, M.; Iriondo, A.; Cambra, J.F.; Gandarias, I.; Jalowiecki-Duhamel, L.; Dumeignil, F.; Arias, P.L. Deactivation Study of the Pt and/or Ni-Based γ-Al_2O_3 Catalysts Used in the Aqueous Phase Reforming of Glycerol for H_2 Production. *Appl. Catal. A Gen.* **2014**, *472*, 80–91. [CrossRef]
61. Zhu, S.; Gao, X.; Zhu, Y.; Zhu, Y.; Zheng, H.; Li, Y. Promoting Effect of Boron Oxide on Cu/SiO_2 Catalyst for Glycerol Hydrogenolysis to 1,2-Propanediol. *J. Catal.* **2013**, *303*, 70–79. [CrossRef]
62. Shi, L.; Yan, P.; Gao, Z.; Huang, W. Effect of Copper Source on the Structure–Activity of $CuAl_2O_4$ Spinel Catalysts for CO Hydrogenation. *Arab. J. Chem.* **2023**, *16*, 104464. [CrossRef]
63. Huang, Z.; Cui, F.; Kang, H.; Chen, J.; Xia, C. Characterization and Catalytic Properties of the CuO/SiO_2 Catalysts Prepared by Precipitation-Gel Method in the Hydrogenolysis of Glycerol to 1,2-Propanediol: Effect of Residual Sodium. *Appl. Catal. A Gen.* **2009**, *366*, 288–298. [CrossRef]
64. Guo, X.; Mao, D.; Lu, G.; Wang, S.; Wu, G. The Influence of La Doping on the Catalytic Behavior of Cu/ZrO_2 for Methanol Synthesis from CO_2 Hydrogenation. *J. Mol. Catal. A Chem.* **2011**, *345*, 60–68. [CrossRef]
65. Águila, G.; Gracia, F.; Araya, P. CuO and CeO_2 Catalysts Supported on Al_2O_3, ZrO_2, and SiO_2 in the Oxidation of CO at Low Temperature. *Appl. Catal. A Gen.* **2008**, *343*, 16–24. [CrossRef]
66. Barbosa, F.F.; Pergher, S.B.C.; Braga, T.P. Synergistic Effects on Cu, Zn and Al-Based Catalyst: Tracking the Change of Active Sites during Glycerol Dehydration. *Braz. J. Chem. Eng.* **2024**, *13*, 1–21. [CrossRef]
67. He, M.; Luo, M.; Fang, P. Characterization of CuO Species and Thermal Solid-Solid Interaction in CuO/CeO_2-Al_2O_3 Catalyst by In-Situ XRD, Raman Spectroscopy and TPR. *J. Rare Earths* **2006**, *24*, 188–192. [CrossRef]
68. Filho, R.W.N.D.; De Araujo Rocha, G.; Montes, C.R.; Vieira-Coelho, A.C. Synthesis and Characterization of Boehmites Obtained from Gibbsite in Presence of Different Environments. *Mater. Res.* **2016**, *19*, 659–668. [CrossRef]
69. Wang, Z.; Tian, Y.; Fan, H.; Gong, J.; Yang, S.; Ma, J.; Xu, J. Facile Seed-Assisted Hydrothermal Fabrication of γ-AlOOH Nanoflake Films with Superhydrophobicity. *New J. Chem.* **2014**, *38*, 1321–1327. [CrossRef]
70. Fang, W.; Liu, S.; Steffensen, A.K.; Schill, L.; Kastlunger, G.; Riisager, A. On the Role of Cu+ and CuNi Alloy Phases in Mesoporous CuNi Catalyst for Furfural Hydrogenation. *ACS Catal.* **2023**, *13*, 8437–8444. [CrossRef]
71. Gao, Y.; Yi, W.; Yang, J.; Jiang, K.; Yang, T.; Li, Z.; Zhang, M.; Liu, Z.; Wu, B. Effect of Calcination Atmosphere on the Performance of Cu/Al_2O_3 Catalyst for the Selective Hydrogenation of Furfural to Furfuryl Alcohol. *Molecules* **2024**, *29*, 2753. [CrossRef]
72. Yano, T.; Ebizuka, M.; Shibata, S.; Yamane, M. Anomalous Chemical Shifts of Cu 2p and Cu LMM Auger Spectra of Silicate Glasses. *J. Electron Spectrosc. Relat. Phenom.* **2003**, *131–132*, 133–144. [CrossRef]
73. Gomes, E.A.; Antunes, R.A.; Mazzer, E.M.; Lins, V. de F.C. High-Temperature Oxidation of Cu–Al–Ni–Mn Shape-Memory Alloy. *Mater. Corros.* **2024**, *75*, 1429–1437. [CrossRef]
74. Yao, Y.; Goodman, D.W. Direct Evidence of Hydrogen Spillover from Ni to Cu on Ni–Cu Bimetallic Catalysts. *J. Mol. Catal. A Chem.* **2014**, *383–384*, 239–242. [CrossRef]

75. Wang, Y.; Zhou, J.; Guo, X. Catalytic Hydrogenolysis of Glycerol to Propanediols: A Review. *RSC Adv.* **2015**, *5*, 74611–74628. [CrossRef]
76. Yfanti, V.L.; Lemonidou, A.A. Mechanistic Study of Liquid Phase Glycerol Hydrodeoxygenation with In-Situ Generated Hydrogen. *J. Catal.* **2018**, *368*, 98–111. [CrossRef]
77. Yfanti, V.L.; Ipsakis, D.; Lemonidou, A.A. Kinetic Study of Liquid Phase Glycerol Hydrodeoxygenation Under Inert Conditions over a Cu-Based Catalyst. *React. Chem. Eng.* **2018**, *3*, 559–571. [CrossRef]
78. Freitas, I.C.; Manfro, R.L.; Souza, M.M.V.M. Hydrogenolysis of Glycerol to Propylene Glycol in Continuous System Without Hydrogen Addition over Cu-Ni Catalysts. *Appl. Catal. B* **2018**, *220*, 31–41. [CrossRef]
79. Mane, R.B.; Rode, C.V. Simultaneous Glycerol Dehydration and In Situ Hydrogenolysis over Cu-Al Oxide Under an Inert Atmosphere. *Green Chem.* **2012**, *14*, 2780–2789. [CrossRef]
80. Cai, F.; Pan, D.; Ibrahim, J.J.; Zhang, J.; Xiao, G. Hydrogenolysis of Glycerol over Supported Bimetallic Ni/Cu Catalysts with and Without External Hydrogen Addition in a Fixed-Bed Flow Reactor. *Appl. Catal. A Gen.* **2018**, *564*, 172–182. [CrossRef]
81. Mendonça, V.G.S.; Freitas, I.C.; Manfro, R.L.; Souza, M.M.V.M. Effect of MgO Addition to Cu-Ni/Al_2O_3 Catalysts on Glycerol Hydrogenolysis in Continuous Reactor Without External Hydrogen. *Appl. Catal. A Gen.* **2022**, *645*, 118838. [CrossRef]
82. Mane, R.B.; Rode, C. V Continuous Dehydration and Hydrogenolysis of Glycerol over Non-Chromium Copper Catalyst: Laboratory-Scale Process Studies. *Org. Process. Res. Dev.* **2012**, *16*, 1043–1052. [CrossRef]
83. Mazarío, J.; Concepción, P.; Ventura, M.; Domine, M.E. Continuous Catalytic Process for the Selective Dehydration of Glycerol over Cu-Based Mixed Oxide. *J. Catal.* **2020**, *385*, 160–175. [CrossRef]
84. Jain, S.R.; Adiga, K.C.; Pal Verneker, V.R. A New Approach to Thermochemical Calculations of Condensed Fuel-Oxidizer Mixtures. *Comb Ustion Flame* **1981**, *40*, 71–79. [CrossRef]
85. Jiménez Correa, M.M.; Aliprandini, P.; Soares Tenório, J.A.; Crocce, D.; Espinosa, R. Precipitation of Metals from Liquor Obtained in Nickel Mining. In *Towards Materials Resource Sustainability*; Springer International Publishing: Berlin/Heidelberg, Germany, 2016; pp. 333–338. ISBN 9783319487687.
86. Hu, W.; Li, W.; Shen, R. Cetyltrimethylammonium Bromide-Promoted, ZnO-Supported, and Mn-Promoted Cu–Fe Catalyst for the Hydrogenation of CO to Low-Carbon Alcohols. *Energy Technol.* **2017**, *5*, 557–567. [CrossRef]
87. Mirzaee, M.; Amini, M.M.; Sadeghi, M.; Mousavi, F.Y.; Sharbatdaran, M. Preparation and Characterization of Boehmite, CuO, TiO_2 and Nb_2O_5 by Hydrothermal Assisted Sol-Gel Processing of Metal Alkoxides. *J. Solgel. Sci. Technol.* **2004**, *31*, 19–23. [CrossRef]
88. Wagner, C.D.; Davis, L.E.; Zeller, M.V.; Taylor, J.A.; Raymond, R.H.; Gale, L.H. Empirical Atomic Sensitivity Factors for Quantitative Analysis by Electron Spectroscopy for Chemical Analysis. *Surf. Interface Anal.* **1981**, *3*, 211–225. [CrossRef]